Atmos. Chem. Phys., 16, 11733–11754, 2016
www.atmos-chem-phys.net/16/11733/2016/
doi:10.5194/acp-16-11733-2016

Atmospheric Chemistry and Physics Open Access EGU

Atmospheric abundance and global emissions of perfluorocarbons CF_4, C_2F_6 and C_3F_8 since 1800 inferred from ice core, firn, air archive and in situ measurements

Cathy M. Trudinger[1], Paul J. Fraser[1], David M. Etheridge[1], William T. Sturges[2], Martin K. Vollmer[3], Matt Rigby[4], Patricia Martinerie[5], Jens Mühle[6], David R. Worton[7], Paul B. Krummel[1], L. Paul Steele[1], Benjamin R. Miller[8], Johannes Laube[2], Francis S. Mani[9], Peter J. Rayner[10], Christina M. Harth[6], Emmanuel Witrant[11], Thomas Blunier[12], Jakob Schwander[13], Simon O'Doherty[4], and Mark Battle[14]

[1]CSIRO Oceans and Atmosphere, Aspendale, Victoria, Australia
[2]Centre for Ocean and Atmospheric Sciences, School of Environmental Sciences, University of East Anglia, Norwich, NR4 7TJ, UK
[3]Laboratory for Air Pollution and Environmental Technology, Empa, Swiss Federal Laboratories for Materials Science and Technology, Dübendorf, Switzerland
[4]School of Chemistry, University of Bristol, Bristol, UK
[5]UJF-Grenoble 1/CNRS, Laboratoire de Glaciologie et Géophysique de l'Environnement, 38041 Grenoble, France
[6]Scripps Institution of Oceanography, University of California at San Diego, La Jolla, California, USA
[7]National Physical Laboratory, Hampton Road, Teddington, Middlesex, TW11 0LW, UK
[8]Cooperative Institute for Research in Environmental Sciences, University of Colorado, Boulder, USA
[9]School of Biological and Chemical Sciences, University of the South Pacific, Suva, Fiji
[10]School of Earth Sciences, University of Melbourne, Australia
[11]UJF-Grenoble 1/CNRS, Grenoble Image Parole Signal Automatique, Grenoble, France
[12]Center for Ice and Climate, Niels Bohr Institute, University of Copenhagen, Copenhagen, Denmark
[13]Climate and Environmental Physics, Physics Institute and Oeschger Centre for Climate Change Research, University of Bern, Bern, Switzerland
[14]Department of Physics and Astronomy, Bowdoin College, Maine, USA

Correspondence to: Cathy M. Trudinger (cathy.trudinger@csiro.au)

Received: 18 May 2016 – Published in Atmos. Chem. Phys. Discuss.: 6 June 2016
Revised: 25 August 2016 – Accepted: 5 September 2016 – Published: 21 September 2016

Abstract. Perfluorocarbons (PFCs) are very potent and long-lived greenhouse gases in the atmosphere, released predominantly during aluminium production and semiconductor manufacture. They have been targeted for emission controls under the United Nations Framework Convention on Climate Change. Here we present the first continuous records of the atmospheric abundance of CF_4 (PFC-14), C_2F_6 (PFC-116) and C_3F_8 (PFC-218) from 1800 to 2014. The records are derived from high-precision measurements of PFCs in air extracted from polar firn or ice at six sites (DE08, DE08-2, DSSW20K, EDML, NEEM and South Pole) and air archive tanks and atmospheric air sampled from both hemispheres. We take account of the age characteristics of the firn and ice core air samples and demonstrate excellent consistency between the ice core, firn and atmospheric measurements. We present an inversion for global emissions from 1900 to 2014. We also formulate the inversion to directly infer emission factors for PFC emissions due to aluminium production prior to the 1980s. We show that 19th century atmospheric levels, before significant anthropogenic influence, were stable at 34.1 ± 0.3 ppt for CF_4 and below detection limits of 0.002 and 0.01 ppt for C_2F_6 and C_3F_8, respectively. We find a significant peak in CF_4 and C_2F_6 emissions around 1940, most likely due to the high demand for aluminium during World War II, for example for construction of aircraft, but these emissions were nevertheless much lower than in recent

Published by Copernicus Publications on behalf of the European Geosciences Union.

years. The PFC emission factors for aluminium production in the early 20th century were significantly higher than today but have decreased since then due to improvements and better control of the smelting process. Mitigation efforts have led to decreases in emissions from peaks in 1980 (CF_4) or early-to-mid-2000s (C_2F_6 and C_3F_8) despite the continued increase in global aluminium production; however, these decreases in emissions appear to have recently halted. We see a temporary reduction of around 15 % in CF_4 emissions in 2009, presumably associated with the impact of the global financial crisis on aluminium and semiconductor production.

1 Introduction

Perfluorocarbons (PFCs) are very potent greenhouse gases (about 7000–11 000 times more powerful than CO_2 on a weight-emitted basis over a 100-year timescale; Myhre et al., 2013). They are very long-lived in the atmosphere, making them of particular relevance for achieving climate stabilisation. We will focus here on three PFCs, CF_4, C_2F_6 and C_3F_8, but there are other PFCs in the atmosphere with lower abundance than CF_4 and C_2F_6 (e.g. Oram et al., 2012; Laube et al., 2012).

CF_4 (carbon tetrafluoride, PFC-14) is the most abundant perfluorocarbon in the atmosphere (Mühle et al., 2010). It is released predominantly from aluminium production (due to so-called "anode effects", when the feed of aluminum oxide to or within the electrolysis cell is restricted; Holiday and Henry, 1959; Tabereaux, 1994) and during semiconductor manufacture (Tsai et al., 2002; Khalil et al., 2003). There is a small natural source from rocks (fluorites and granites) released by tectonic activity and weathering (Harnisch and Eisenhauer, 1998; Deeds et al., 2008, 2015; Mulder et al., 2013; Schmitt et al., 2013). Other very small industrial sources of CF_4 include release during production of SF_6 and HCFC-22 (Institute for Environmental Protection and Research, 2013) and from UV photolysis of trifluoroacetyl fluoride, which is a degradation product of halocarbons such as HFC-134a, HCFC-124 and CFC-114a (Jubb et al., 2015). Another possible source of CF_4 is from the rare earth industry, particularly in China, specifically neodymium oxide electrolysis (Vogel and Friedrich, 2015). However, these other sources of emissions have been negligible to date compared to the CF_4 emissions due to aluminium production and semiconductor manufacture (Harnisch and Eisenhauer, 1998; Jubb et al., 2015; Wong et al., 2015).

C_2F_6 (perfluoroethane, PFC-116) is released predominantly during aluminium production and semiconductor manufacture (Tsai et al., 2002; Fraser et al., 2013). It is also used in the R-508 refrigerant blend, although emissions are believed to be small compared to the other sources (Kim et al., 2014). C_3F_8 (perfluoropropane, PFC-218) is the least abundant of these three PFCs and is used as a refrigerant as well as being released during semiconductor manufacture (EDGAR, 2010; Tsai et al., 2002). C_3F_8 has been detected at low levels in emissions from aluminium smelters (Fraser et al., 2013; Li et al., 2012). The aluminium industry does not currently account for C_3F_8 emissions (International Aluminium Institute, 2014) or include them in the current IPCC guidelines for bottom up accounting of PFC emissions from aluminium production (IPCC, 2006), but due to the low levels compared to the other PFCs (Fraser et al., 2013; Li et al., 2012) C_3F_8 is likely to be difficult to detect with the measurement systems used by the aluminium industry. Natural sources of C_2F_6 and C_3F_8 have not been identified (Harnisch, 1999).

Sinks of these PFCs are dominated by unintentional thermal destruction during high-temperature combustion at ground level, giving atmospheric lifetimes for CF_4, C_2F_6 and C_3F_8 of about 50 000, 10 000 and 2600 years, respectively (Cicerone, 1979; Morris et al., 1995; Myhre et al., 2013). PFCs have been targeted by both the aluminium and semiconductor industries for emission controls to reduce greenhouse gas emissions.

Atmospheric measurements of greenhouse gases are the only reliable way to verify estimates of global emissions to ensure that we can predict the effect of emissions on radiative forcing and to guide mitigation options. Mühle et al. (2010) gave a summary of previous measurements of CF_4, C_2F_6 and C_3F_8, then presented new high-precision measurements from 1973 to 2008 on air from (a) the Cape Grim Air Archive (Langenfelds et al., 1996), (b) a suite of tanks with old northern hemispheric air and (c) the Advanced Global Atmospheric Gases Experiment (AGAGE) in situ atmospheric monitoring network. They presented estimates of global trends in PFC abundance and the corresponding emissions from 1973 to 2008. They showed that global emissions peaked in 1980 (CF_4) or early-to-mid-2000s (C_2F_6 and C_3F_8) before decreasing due to mitigation efforts by both the aluminium and semiconductor industries. The emissions estimates based on atmospheric measurements were significantly higher than previous estimates based on inventories. Kim et al. (2014) extended this work using measured C_2F_6 / CF_4 emission ratios specific to the aluminium and semiconductor industries to partition global emissions to each industry. They suggested that underestimated emissions from the global semiconductor industry during 1990–2010 and China's aluminium industry after 2002 accounted for the discrepancy between PFC emissions based on atmospheric measurements and inventories. Underestimated PFC emissions may also be from previously unaccounted-for emissions from aluminium production due to undetected anode effects (Wong et al., 2015).

Air extracted from firn (the layer of unconsolidated snow overlying an ice sheet) or bubbles in polar ice provides a reliable way to reconstruct atmospheric composition prior to direct atmospheric measurements. Mühle et al. (2010) estimated the pre-industrial, natural background abundances

from firn air at the Megadunes site in Antarctica (air with a mean age of about AD 1910) and air from 11 samples of melted glacial ice at Pâkitsoq in Greenland (with ages between 19 000 and 11 360 BP) to be 34.7 ± 0.2 ppt for CF_4 (based on both Megadunes and Pâkitsoq) and 0.1 ± 0.02 ppt for C_2F_6 (based on Megadunes alone). Worton et al. (2007) used firn measurements from the North Greenland ice core project site (NGRIP) and Berkner Island, Antarctica, to reconstruct CF_4 from the mid-1950s and C_2F_6 from 1940 to present. However, these previous records from firn and ice are not continuous through from pre-industrial to recent levels.

Here we present measurements of CF_4, C_2F_6 and C_3F_8 in air extracted from four firn sites (DSSW20K, EDML, NEEM 2008 and South Pole 2001) and two ice cores (DE08 and DE08-2). We combine these with the air archive and in situ measurements from Mühle et al. (2010), extended to the end of 2014, and use an inversion calculation to estimate global emissions, with uncertainties, and show how these PFCs have varied in the atmosphere from pre-anthropogenic levels in the 19th century to 2014. We also reformulate our inversion to directly infer emission factors for PFC emissions due to aluminium production for the period up to 1980 when aluminium production dominates PFC emissions.

2 Methods

2.1 Data – locations, measurement and calibration scales

The firn and ice core measurements used in this work come from ice or firn air collected at the following sites:

- DE08 and DE08-2 are located 16 km east of the summit of Law Dome (66.7° S, 112.8° E) in East Antarctica (Etheridge et al., 1996, 1998). They are 300 m apart and have nearly identical site characteristics, including very high snow accumulation rates ($1100\,kg\,m^{-2}\,yr^{-1}$). Ice cores were drilled at DE08 and DE08-2 in 1987 and 1993, respectively.

- DSSW20K is 20 km west of the deep DSS (Dome Summit South) drill site near the summit of Law Dome in East Antarctica (Smith et al., 2000; Sturrock et al., 2002; Trudinger et al., 2002). DSSW20K has a short firn column and a moderate snow accumulation rate ($150\,kg\,m^{-2}\,yr^{-1}$). Firn air was collected in January 1998.

- EDML (EPICA Dronning Maud Land) is the EPICA drill site near Kohnen Station (75.2° S, 0.1° E), in Dronning Maud Land, Antarctica (Weiler, 2008; Mani, 2010). It has a low snow accumulation rate ($65\,kg\,m^{-2}\,yr^{-1}$) and firn air was collected in January 2006.

- NEEM 2008 firn air was extracted from a borehole near the NEEM (North Greenland Eemian Ice Drilling Project) deep ice core drilling site (77.5° N, 51.1° W) in northern Greenland (Buizert et al., 2012). NEEM has a moderate snow accumulation rate ($199\,kg\,m^{-2}\,yr^{-1}$). We use air from the EU borehole collected in July 2008.

- South Pole 2001, Antarctica (90° S), has a deep firn and a low snow accumulation rate ($74\,kg\,m^{-2}\,yr^{-1}$) (Butler et al., 2001; Aydin et al., 2004; Sowers et al., 2005). Here we measure only one sample from the South Pole, collected in 2001 from 120 m.

In addition to the firn and ice core measurements, we use archived and in situ measurements from Mühle et al. (2010), extended to the end of 2014 and focused on the high latitudes in each hemisphere.

Measurements were made using two different measurement systems and primary calibration scales. The measurements in Mühle et al. (2010) were made on Medusa systems (Miller et al., 2008) and reported on Scripps Institution of Oceanography (SIO) primary calibration scales (SIO-05 for CF_4 and SIO-07 for C_2F_6 and C_3F_8). Measurements of firn air from DSSW20K, NEEM 2008 and South Pole 2001 were made at CSIRO (Aspendale) or Cape Grim on the Medusa system and are also reported on SIO calibration scales. Air was extracted from DE08 and DE08-2 ice in ICELAB at CSIRO (Aspendale) using a "cheese grater" dry extraction system (Etheridge et al., 1988). Air from the DE08 and DE08-2 ice cores and the EDML firn was analysed at the University of East Anglia (UEA) using high-sensitivity gas chromatograph/trisector mass spectrometer system (Waters/Micromass Autospec) (Worton et al., 2007; Sturges et al., 2001; Mani, 2010). Measurements made at UEA are reported on UEA calibration scales. We derive conversion factors between the two calibration scales in Appendix A and report all measurements on the SIO-05 (CF_4) and SIO-07 (C_2F_6 and C_3F_8) primary calibration scales. Further measurement details are available in Appendix B. The firn, ice core and archive measurements are available in the Supplement. The in situ measurements are available on the CDIAC website (Prinn et al., 2016).

2.2 Firn model

To characterise the age of the air in the firn and ice samples, we use a numerical model of the processes that occur in firn and ice (mainly diffusion of air in the firn layer, advection of snow downwards as new snow falls at the surface and gradual trapping of the air into bubbles). These processes mean that air contained in firn or ice corresponds to atmospheric air over a range of times rather than a single age. We use the CSIRO firn model (Trudinger et al., 1997), updated by Trudinger et al. (2013), and the LGGE-GIPSA firn model (Witrant et al., 2012) to characterise the air age and

age spread. We use the two independent models as a way to incorporate firn model uncertainty.

The depth profile of diffusivity in the firn and other diffusivity-related parameters in the firn models need to be calibrated for each site that we model. To do this we tune the models to fit firn measurements of trace gases for which we know the past atmospheric history. Calibration of the CSIRO firn model for DE08 and DE08-2 (which are modelled as identical sites), as well as DSSW20K, NEEM 2008 and South Pole 2001, is described in Trudinger et al. (2013), and for EDML in Appendix C. Calibration of the LGGE-GIPSA model is described in Witrant et al. (2012) for all sites except EDML and DSSW20K, which are described in Appendix C. Note that although only one South Pole sample (from 120 m) was analysed for PFCs in our study, calibration of diffusivity at South Pole in both firn models was based on measurements throughout the entire depth profile.

The diffusion coefficients we use for the PFCs relative to CO_2 (for temperature of 244.25 K and pressure of 745 mb) are 0.823 for PFC-14 (Buizert et al., 2012, based on measurements by Matsunaga et al., 2005) and 0.583 and 0.497 for PFC-116 and PFC-218, respectively (using Le Bas molecular volumes; Fuller et al., 1966). The uncertainty in relative diffusion coefficients based on measurements by Matsunaga et al. (2005) is about 2 % and about 5–10 % from other methods (based on discrepancies between different estimates; Martinerie et al., 2009; Buizert et al., 2012; Trudinger et al., 2013).

As the firn model is linear, and the physical processes in firn are taken as constant in time, we can characterise the firn models using Green's functions (also known as age distributions, age spectra or pulse response functions) that relate the mole fraction of a trace gas at the measurement depths to atmospheric mole fraction of that gas over a range of times (Rommelaere et al., 1997; Trudinger et al., 2002). We denote these Green's functions as $G_{a\rightarrow i}$, as they represent the effect of atmospheric mole fraction in each year on mole fraction at a particular depth in ice or firn, with "a" for atmosphere and "i" for ice (or firn). The Green's functions change shape with depth through the firn layer, widening with increasing depth, but their shape does not change with depth for bubbles trapped in ice (assuming stationary conditions associated with relatively stable climate). Green's functions from the firn model, shown for DSSW20K in Fig. 1a, will be used as described in the next section.

In order to incorporate the effect of uncertainty in the firn models into our inversion calculations, we use an ensemble of Green's functions for each site, constructed as follows. When we calibrate the CSIRO firn model, in addition to finding the diffusivity profile that gives the best fit to calibration observations, we also create some alternative diffusivity profiles that approximately represent the 95 % confidence interval of the firn model parameters, as described by Trudinger et al. (2013). In some cases we also include Green's functions generated with the CSIRO model using different formulations of model processes (e.g. convective mixing near the surface at DSSW20K is modelled with exponentially decreasing eddy diffusion or with a well-mixed layer). We select between four and seven Green's functions for each site from the CSIRO model, and add one or more Green's functions from the LGGE-GIPSA model obtained from the analytical method presented in Witrant and Martinerie (2013), to represent the variation in the complete ensemble for each firn/ice site. We repeat the inversion calculation with all combinations of Green's functions for each site, giving more than 1300 combinations for the five firn/ice sites considered in this study. We also include Green's functions calculated with the CSIRO model using our best diffusivity profile but with relative diffusion coefficients that are ±5 % (for CF_4) or ±10 % (for C_2F_6 and C_3F_8) of the values given above (with relative diffusion coefficients used consistently across all sites at once).

2.3 Inversion calculations

We begin with an inversion of the air archive and in situ PFC measurements at the monthly timescale and semi-hemispheric spatial scale, to infer emissions of CF_4 and C_2F_6 from 1978 to 2014 and C_3F_8 from 1983 to 2014 (the inversion for C_3F_8 starts later than the other two because the early archive C_3F_8 measurements are particularly scattered). Initial mole fraction in 1978 (or 1983 for C_3F_8) is also estimated. This inversion will be referred to as the "InvE1" inversion and is very similar to the inversion given in Mühle et al. (2010), but with an updated inversion method (Rigby et al., 2011, 2014) and with observations extended to the end of 2014. The InvE1 inversion uses the 2-D 12-box AGAGE atmospheric transport model (Cunnold et al., 1994; Rigby et al., 2013) to calculate the mole fraction of the PFCs in each semi-hemisphere from emissions. The 12-box model has four boxes north–south by three boxes in the vertical, with boundaries at 30° N, 0° and 30° S in the horizontal and 500 and 200 hPa in the vertical.

We then use an inversion similar to Trudinger et al. (2002) to infer emissions at the annual timescale from the ice core, firn, archive and in situ measurements from 1900 to 2014. This inversion will be referred to as the "InvE2" inversion. InvE1 is the most appropriate inversion for the in situ and archive part of the record, while InvE2 was developed to focus on the issues associated with inverting firn and ice core measurements. InvE2 will be described in detail here; details of InvE1 are given in the references listed above. InvE2 also uses the AGAGE 12-box atmospheric transport model, mainly for consistency with InvE1.

The firn and archive data do not have adequate information content to constrain semi-hemispheric emissions, so InvE2 infers annual global emissions with a fixed north–south distribution (for this we use the estimated north–south distribution from InvE1 for 1990). The AGAGE 12-box model is used to relate annual high-latitude mole fraction in each

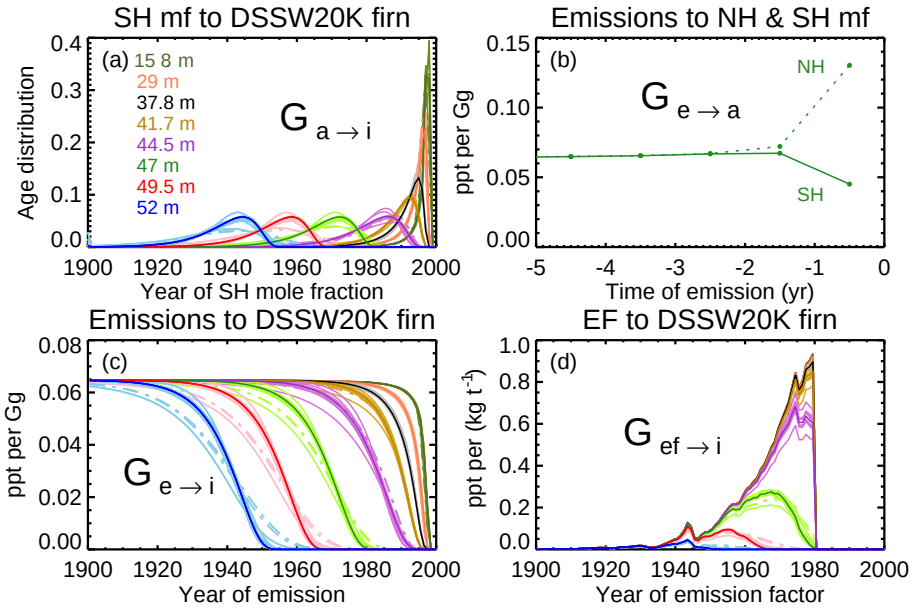

Figure 1. **(a)** Green's functions ($G_{a\rightarrow i}$) relating the mole fraction at DSSW20K measurement depths to high-latitude southern hemispheric (SH) atmospheric mole fraction, from the firn models, with different colours for each depth. The dark coloured lines show the preferred Green's functions from the CSIRO model, while the lighter coloured lines show the other members of the ensemble of Green's functions, with the Green's functions from the LGGE-GIPSA firn model shown with the dot-dashed lines. **(b)** Green's functions ($G_{e\rightarrow a}$) describing the relationship between atmospheric mole fraction in ppt in the high-latitude Northern Hemisphere (NH, dashed line) and high-latitude Southern Hemisphere (solid line) and annual global CF_4 emissions in Gg in preceding years, from the AGAGE 12-box model based on the spatial emissions distribution described in the text. We define mole fractions to correspond to the start of the year and emissions to correspond to the middle of the year. The x axis gives the time of emission relative to the time of atmospheric mole fraction. **(c)** Green's functions ($G_{e\rightarrow i}$) relating the mole fraction at DSSW20K measurement depths to annual global CF_4 emissions, derived by combining the Green's functions in parts **(a)** and **(b)**. Line styles and colours are as in **(a)**. **(d)** Green's functions ($G_{ef\rightarrow i}$) relating the mole fraction at DSSW20K measurement depths to annual global CF_4 emission factor in $kg\,t^{-1}$, derived by combining the Green's functions in part **(c)** with annual global primary aluminium production up to 1980. Line styles and colours are as in **(a)**.

hemisphere to annual global emissions with the fixed north–south distribution, creating Green's functions that are denoted $G_{e\rightarrow a}$, with "e" for emissions and "a" for atmosphere (Fig. 1b). InvE2 uses Green's functions that relate measured firn or ice core mole fractions to annual global emissions. We create these Green's functions (which will be denoted $G_{e\rightarrow i}$, Fig. 1c) by multiplying the $G_{e\rightarrow a}$ Green's functions with the $G_{a\rightarrow i}$ Green's functions described earlier. The observations used in InvE2 are firn and ice core measurements plus high-latitude mole fraction in each hemisphere at annual resolution, obtained by fitting a smoothing spline to the archive and in situ measurements and sampling as described in Appendix D. InvE2 starts from equilibrium (pre-anthropogenic) conditions, so the initial mole fractions are set to the pre-anthropogenic background levels that we estimate from our measurements.

We may expect to see a shift in the north–south distribution of emissions over time in recent decades, when global emissions have gone from being predominantly due to aluminium production to now include semiconductors and as developing nations such as China have increased their fraction of global emissions. InvE1 is capable of estimating such a shift in emissions, although with the caveat that derived emissions at the semi-hemispheric level are known to be sensitive to uncertainties in the model transport parameters. Use of a constant north–south distribution of emissions in InvE2 is the best choice prior to the 1980s when the emissions distribution was probably more stable than in recent decades, and the firn and ice core measurements would not contain adequate information to resolve distribution changes anyway. However, use of the constant emissions distribution does degrade the fit to observations in recent decades. We can use the emissions distribution already estimated by InvE1 to improve InvE2. We do this by subtracting the (modelled) contribution to all mole fraction measurements of the monthly semi-hemispheric emissions after 1980 inferred from InvE1, before inverting for additional emissions with the constant north–south gradient. These additional emissions estimated by InvE2 will mostly be emissions before 1980, although they could include small adjustments (positive or negative) to the emissions after 1980, but the adjustments will have the constant (1990) spatial distribution. In this way, we are combining the strengths of the higher-resolution InvE1 inversion for the monthly in situ measurements with the InvE2 inver-

sion for the ice, firn and early archive measurements, to give our best estimate for emissions.

Because primary aluminium production is known much more precisely than emission factor for the PFCs, we also formulate the inversion to directly estimate PFC emission factors (in kilograms per metric tonne, $\mathrm{kg\,t^{-1}}$) from aluminium production before the mid-1980s, assuming that aluminium production is the dominant source for this period. This inversion will be denoted "InvEF". We create new Green's functions that relate measured high-latitude mole fraction to emission factor, $G_{\mathrm{ef}\rightarrow\mathrm{i}}$ with ef for emission factor (Fig. 1d), by multiplying the $G_{\mathrm{e}\rightarrow\mathrm{i}}$ Green's functions by global primary aluminium production in each year (using estimates from the U.S. Geological Survey (2014) and International Aluminium Institute (2014), shown by the grey line in Fig. 2e).

For the InvEF inversion, we first subtract from the observations the effect of the InvE1 emissions after a selected date ($T_1 = 1985$ for CF_4 and C_2F_6, and 1988 for C_3F_8), then estimate emission factor only up to the date T_1. We need to do this because emissions in recent decades were not only due to aluminium production, with semiconductor emissions making a significant contribution to global emissions. T_1 is chosen to be 5 years after the beginning of the InvE1 inversion, to avoid the effect of initialisation of mole fraction on the emissions inferred by InvE1 (see Sect. 3.2). The period up to T_1 is most likely dominated by emissions due to aluminium production, but if there is a significant contribution from other sources, this would lead to emission factors that are too high. EDGAR 4.1 (EDGAR, 2010) estimates that aluminium production was responsible for at least 99 % of CF_4 emissions up to 1985, and 90 % of C_2F_6 emissions in 1985 (down from 99 % in 1972). C_3F_8 emissions estimates in EDGAR 4.1 for all sources before 1988 are much smaller than the emissions implied by the atmospheric measurements (Mühle et al., 2010), so it is difficult to be sure about the contribution of different C_3F_8 sources before 1988, but we would expect it to be similar to CF_4 and C_2F_6. Our interpretation of the emission factor results needs to keep in mind the possibility of sources other than aluminium production for the entire period up to T_1, but the EDGAR emissions estimates have suggested particular care with emission factors for C_2F_6 between 1972 and 1985.

2.3.1 Uncertainties and regularisation in the inversion calculations

There are a number of contributions to the uncertainties in inferred emissions and atmospheric abundance (Trudinger et al., 2002). The most obvious contributions are data error (analytical, calibration scale, sampling uncertainties) and model error. In our case, model error can be due to the firn model (from missing or incorrectly modelled processes and uncertainty in model parameters), as well as the atmospheric model that relates emissions to mole fraction. To capture

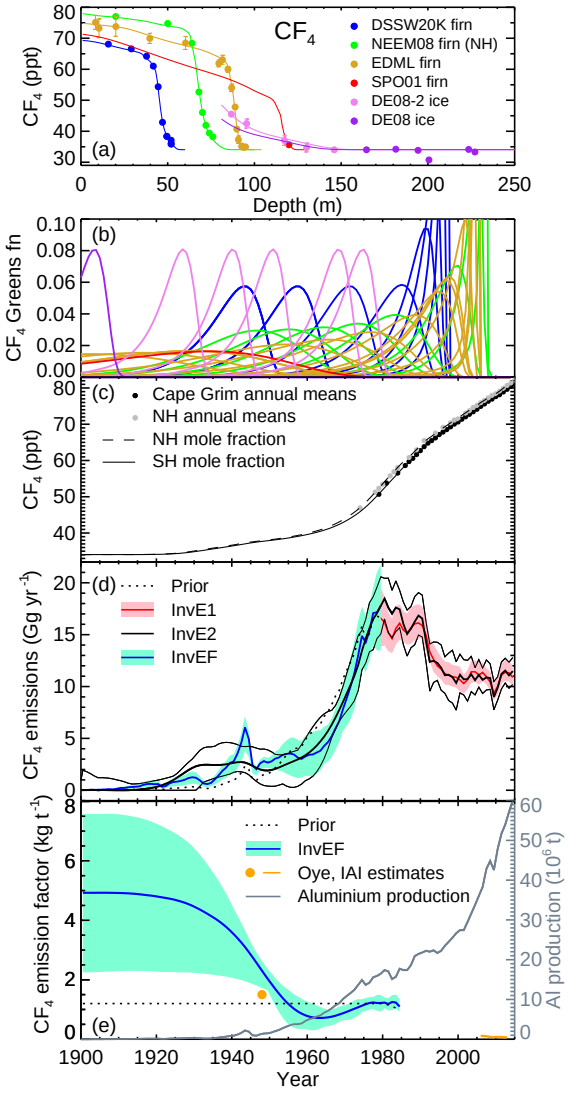

Figure 2. **(a)** Depth profiles of CF_4 mole fraction in the firn and ice. Lines show model results corresponding to inferred emissions from InvE2; symbols are measurements with 1σ uncertainties. **(b)** Green's functions from the CSIRO firn model (colours correspond to those in panel **a**). **(c)** Time history of mole fraction in the Northern Hemisphere (NH, dashed line) and Southern Hemisphere (SH, solid line) calculated with emissions inferred by InvE2. Symbols show annual values determined from atmospheric measurements in each hemisphere. **(d)** Emissions inferred from the three inversions, with 95 % confidence intervals. The dotted line shows the prior estimate based on a constant emission factor. **(e)** Emission factor inferred by the InvEF inversion with 95 % confidence intervals (blue) and constant prior (dotted). Emission factor estimated by Oye et al. (1999) for 1948 (orange circle) and recent estimates by the International Aluminium Institute (2014) (orange line, lower right corner). Primary aluminium production (U.S. Geological Survey, 2014; International Aluminium Institute, 2014) in 10^6 t (million metric tonnes) is shown with the grey line (right axis).

the firn model uncertainty, we use an ensemble of Green's functions, from two firn models, as mentioned above. We assume that errors in the atmospheric model at the annual timescale for global emissions would be significantly smaller than other contributions to the error.

The contribution to the error that is most difficult to deal with is due to the fact that we are solving an inverse problem that is ill-conditioned, so that the solution is not unique. In our case, the ill-conditioning is partly due to lack of data (mole fraction in the firn is not known at all depths) but also importantly it is a consequence of the smoothing (and therefore lost information) by the firn and bubble trapping processes. As noted by Rommelaere et al. (1997), an atmospheric event of period shorter than the width of the Green's function is unlikely to be resolved in firn or ice core data. Therefore, when we invert a firn depth profile, the information contained in the firn data does not constrain variations in the atmospheric mole fraction at high (e.g. annual) frequencies. Rommelaere et al. (1997) demonstrated for CO_2 that atmospheric histories with wild (and unrealistic) oscillations can be consistent with the firn measurements (as long as high and low events counteract each other and have periods that are short relative to the Green's function width), but our knowledge of the budget of trace gases often excludes such possibilities. This budget knowledge needs to be incorporated into the inversion somehow, or the uncertainty in annual emissions will be unrealistically high and may therefore not be useful.

Regularisation (e.g. minimising the length of the solution; Menke, 1989) was used by Rommelaere et al. (1997) to address the problem of ill-conditioning. The use of prior information on either mole fractions or emissions can also help. Rigby et al. (2011) used prior information on the rate of change of emissions, rather than the absolute magnitude, as often the timing of changes in emissions is known even if the estimated magnitude may be incorrect. Constraints can also help, such as non-negativity constraints on emissions or mole fraction for long-lived gases (Trudinger et al., 2002). However, once constraints like these are used, the inversion, which originally was linear, usually becomes nonlinear. Another method is to smooth the solution and its uncertainties (e.g. running mean), taking into account the strong anticorrelations between uncertainties in adjacent years, then report the smoothed solution and smoothed uncertainties, as done by Trudinger et al. (2002). It would also be possible to infer mole fraction or emissions at lower frequencies (e.g. decadal averages rather than annual values), but we might then miss out on information about trends within decades that is available in the data when we incorporate our understanding of the budget, and we would need to be careful about temporal aggregation error (Thompson et al., 2011). Each of these methods to deal with the uncertainty due to ill-conditioning has different advantages and disadvantages and it is important to understand the consequences of any choices.

In the InvE2 and InvEF inversions, we use regularisation similar to Rommelaere et al. (1997) to avoid unrealistic oscillations by including a term in the cost function to be minimised that is the sum over all years of the change from one year to the next in emissions (or emission factor). This term is weighted in the cost function by a parameter, α. We need to choose α so that it suppresses unrealistic oscillations but does not smooth out too much of the real year-to-year variation in emissions that we are interested in. We also use a constraint that emissions and emission factors must not be negative.

Uncertainties in estimated emissions are calculated by repeating the inversion many times with perturbations to model inputs, including (a) firn model Green's functions, (b) observations perturbed according to their uncertainty, as in bootstrapping (Efron and Tibshirani, 1993), (c) initial mole fraction and (d) the period for which the spatial distribution of emissions is taken from the InvE1 inversion. We calculate the uncertainties due to each contribution separately, only to see the relative contributions. To calculate the total uncertainty we perturb all inputs at once and take the full range of emissions to represent the 95 % confidence interval of emissions and the full range of the corresponding mole fractions to represent the 95 % confidence interval for atmospheric mole fraction. If we were to combine the uncertainties from the individual contributions in quadrature to calculate total uncertainties, we could end up with negative emissions being included in the uncertainty range for part of the time period, which would imply that the uncertainty range was too large. We wish to stay consistent with the constraints provided by the measurements and ensure emissions are not negative. This is likely to give an uncertainty range that is not symmetric about the best solution when the best solution is near zero. Separately we also test the sensitivity of results to leaving out the observations from each site one at a time, as well as the parameter α that gives the weight of the smoothness constraint in the cost function.

Apart from the regularisation term involving the year-to-year changes in emissions (or emission factor), the cost function consists of the squared model–data mismatch weighted by the observation uncertainties. We do not include the prior estimate in the cost function. Previous studies (Mühle et al., 2010; Kim et al., 2014) found that bottom-up estimates of PFC emissions were too low, and we did not want these to bias our results. A prior estimate is, however, used as a starting point for the inversion calculation. The InvE2 and InvEF inversions are implemented in IDL (Exelis Visual Information Solutions, Boulder, Colorado) using the *constrained_min* routine.

Prior emissions for the InvE2 inversion after 1980 (or 1983 for C_3F_8) are taken as zero (because we subtract the effect of the InvE1 emissions from the measurements). Prior emissions before 1980 (or 1983) are based on emissions calculated by multiplying estimates for global primary aluminium production by an emission factor (kg PFC/tonne Al

produced) determined as follows. For CF_4, we use a constant emission factor of 1.2 kg t^{-1}, chosen to match the InvE1 emissions in 1980. We could have increased the emission factor back in time – for example, Oye et al. (1999) suggested an emission factor of 1.5 kg t^{-1} in 1948 – but as the prior estimate is used only as a starting point for the inversion we chose the simplest option. We take the emission factor for C_2F_6 to be 0.13 kg t^{-1} (95 % of InvE1 emissions divided by aluminium production, because EDGAR 4.1 has C_2F_6 emissions due to aluminium production contributing about 95 % of the total emissions in 1980), also assumed to be constant in time. For C_3F_8, we use an emission factor of 0.01 kg t^{-1}, based on the InvE1 emissions in 1983, assumed constant with time.

3 Results

3.1 Inversion results

Figures 2, 3 and 4 show inputs and results for CF_4, C_2F_6 and C_3F_8 for all three inversion calculations (InvE1, InvE2 and InvEF). In each case, the first panel shows the firn and ice core measurements and the modelled depth profiles that correspond to emissions calculated by the InvE2 inversion (using observations from all sites at once). The second panel shows Green's functions from the CSIRO firn model that relate the mole fraction at the firn and ice core measurement depths to either northern or southern hemispheric high-latitude atmospheric mole fraction ($G_{a\rightarrow i}$). Each line corresponds to one measurement depth and shows the estimated proportion of the measured PFC mole fraction in that firn or ice core sample that comes from the overlying atmosphere in each year. The Green's functions are narrowest at DE08 and DE08-2, second narrowest at DSSW20K, intermediate width at NEEM and widest at the South Pole and EDML. Depths with measured mole fraction that are below detection limits (for C_2F_6 and C_3F_8) have Green's functions shown with dashed lines. When the measured mole fraction is zero (or below detection), we can assume that the atmospheric mole fraction for the years covered roughly by the Green's function for that depth had zero or very low mole fraction (Trudinger et al., 2002), give or take a few years for uncertainty in the Green's function and how high the atmospheric mole fraction would need to be during the years near the edge of the Green's function to cause detectable mole fraction in the firn. The Green's functions in the second panel provide the link between the first and third panels and show the significant overlap of Green's functions at different depths and sites.

The third panel shows the estimated history of PFC mole fraction in the atmosphere for the high-latitude northern (dashed) and southern (solid) latitudes calculated with the InvE2 inferred emissions. The annual values of atmospheric PFC mole fraction that are used in the inversion are shown by

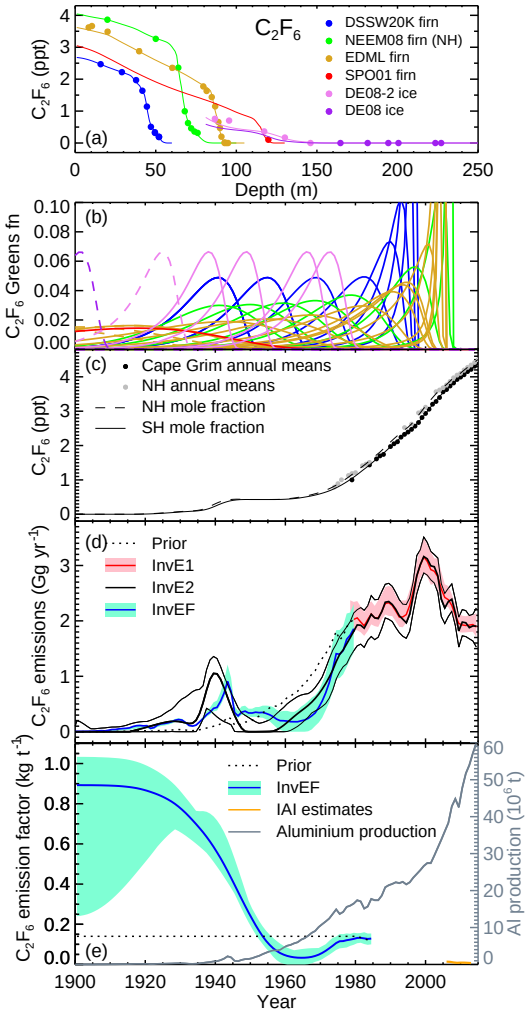

Figure 3. Inputs and results for the C_2F_6 inversions. Panels, line styles and symbols are as in Fig. 2, except that Green's functions in **(b)** are dashed if the measured mole fraction is zero (or below detection).

the black circles for the Southern Hemisphere (based on the Cape Grim air archive and in situ data) and the grey circles for the Northern Hemisphere (based on northern hemispheric tanks and Mace Head in situ data).

The fourth panel shows the emissions estimated by the three inversions. The red, inner black and blue lines show our preferred solution for each inversion. The pink shading, outer black lines and blue shading show the estimated 95 % confidence intervals. The InvEF inversion estimates emission factors, and we combine the inferred emission factor with aluminium production to calculate the corresponding emissions that are shown here. For InvE2 and InvEF, the confidence intervals come from the full ensemble of Green's functions plus other components of the uncertainty as described in Sect. 2.3.1. The dashed grey lines show the prior emissions

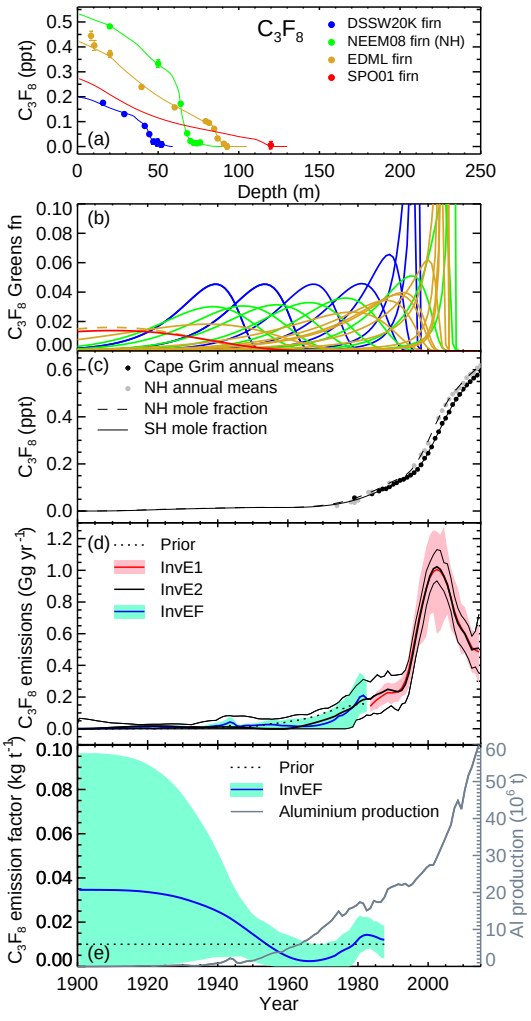

Figure 4. Inputs and results for the C_3F_8 inversions. Panels, line styles and symbols are as in Fig. 3.

before 1980 constructed from aluminium production and the constant emission factor.

The fifth panel shows emission factors inferred by the InvEF inversion, with 95 % confidence intervals. We also show estimates of recent CF_4 and C_2F_6 emission factor from the International Aluminium Institute (2014) (orange line, lower right corner) and the CF_4 emission factor estimate for 1948 from Oye et al. (1999). Reconstructed histories of mole fraction, emissions and emission factor are available in the Supplement.

Our inversions simultaneously match almost all firn and ice core measurements very well, showing consistency between the different sites and between the firn, ice core and atmospheric observations. Our inferred emissions between 1975 and 2008 are very much like those in Mühle et al. (2010). They are based on essentially the same data, and the small differences would mainly be due to choices in the different inversion calculations. The peaks in emissions around 1980 (CF_4) or early-to-mid-2000s (C_2F_6, C_3F_8), followed by decreases in emissions, are prominent features in the records and have already been described in detail by Mühle et al. (2010). The firn and ice core measurements have shown quite stable mole fraction levels in the early 20th century, followed by peaks in CF_4 and C_2F_6 emissions around 1940, then strong increases in emissions from around 1960 in all three PFCs. The estimated emission factors are quite high in the first few decades of the 20th century. We will discuss these features of the reconstructions in more detail in Sect. 4; in the remainder of Sect. 3 we will look in more detail at the inversion calculations.

3.2 Comparison of different inversions

The emissions from the InvE2 inversion are very similar to those from the InvE1 inversion. The only notable differences are that the InvE2 inversions for CF_4 and C_3F_8 give higher emissions in the early 1980s, but this is when the InvE1 inversion is just beginning, and it depends on the oldest samples in the archive records and could be subject to end-effects including potential aliasing of the emissions with the initial conditions. It is due to these differences that we have chosen the start date for the emission factor inversion, T_1, to be 5 years later than the start of the InvE1 inversion.

The estimated emissions from InvEF are generally quite similar to those from InvE2, but there are significant differences in the temporal variability. It is important to note that in InvE2, regularisation is applied to emissions (minimising the year-to-year variability in emissions along with the model–data mismatch, as described in Sect. 2.3.1), whereas in InvEF, regularisation is applied to the emission factor. This has implications for the temporal variability in the two different inversions. Temporal variability in aluminium production is directly reflected in the emissions from the InvEF inversion (emissions are the product of the inferred emission factor and aluminium production). Although the variation in estimated CF_4 emission factor through the 1940s is quite smooth (Fig. 2e), the peak in aluminium production in the 1940s is not smooth, and it gives quite a prominent peak in CF_4 emissions from InvEF at this time (Fig. 2d). We would be less likely to see the same structure in the emissions in InvE2 around 1940, firstly because such rapid variation is unlikely to survive smoothing due to the firn processes to be recoverable in such detail from the firn or ice core measurements, but also the regularisation would penalise solutions with rapid variability in emissions like this. The aim of regularisation is to remove any variations that are too rapid to be resolved in the firn or ice, so these two reasons are related. We do, however, see a relatively sharp peak around 1940 in C_2F_6 emissions in Fig. 3d. There are physical reasons for expecting the emission factor to vary more slowly than emissions – the emission factor is likely to depend on the current technology used to produce aluminium, which presumably will change more slowly than aluminium production itself which needs

to respond rapidly to demands. For this reason, we favour the variability in emissions from the InvEF inversion, with emissions reflecting the product of the slower change in emission factor with the more rapid change in aluminium production.

The estimated emission factors are quite high in the first few decades of the 20th century, but this is multiplied by very small aluminium production, leading to small emissions. The uncertainty in emission factor in this period is large and is dominated by the assumed background mole fraction levels. Our estimated CF_4 emission factor of 1.8–2.7 kg t^{-1} in 1948 is larger than the 1.5 kg t^{-1} estimated by Oye et al. (1999). Recall that the emission factor for C_2F_6 after 1970 might be overestimated if there are significant emissions of C_2F_6 due to semiconductors at this time. Our estimated emission factors were based on the assumption that aluminium production was the only source for these PFCs before the early 1980s. While we know that this was probably not quite true at the end of the period, we believe it to be true before about 1970. We are not aware of sources of PFCs other than aluminium production that are likely to have been significant before 1970.

3.3 Sensitivity studies

Figure 5a shows the sensitivity of the inferred CF_4 emissions from InvE2 to excluding each of the measurement sites (including the Cape Grim and northern hemispheric atmospheric measurements). Exclusion of DE08-2 is the only site that makes a difference to the estimated emissions before 1955, and we see a more gradual increase in emissions from 1900 without DE08-2 rather than the increase from 1920 that the DE08-2 measurements imply. DE08-2 is the site with the narrowest age distributions, and the oldest DE08-2 measurement is centred around the 1920s (Fig. 2b). DE08 has age distributions with the same width as DE08-2 but older air and no samples containing air after 1910. The resolution and timing of the DE08-2 ice core measurements are valuable to these calculations. We do not currently have measurements of C_3F_8 in the DE08 or DE08-2 ice cores. If we did, the extent to which they would improve the temporal resolution of the estimated C_3F_8 emissions is likely to depend on their uncertainty and the measurement detection limit.

Figure 5b shows CF_4 emissions from InvE2 for different values of the regularisation parameter α. For the low values we see an increase in the variability, while for the high values we see that the emissions peak around 1980 starts to be suppressed. Interestingly, for lower values of α we get a higher peak in the early 1940s, coinciding with the peak in aluminium production. Our choice of α generally seems a reasonable one to suppress unrealistic variation while retaining much of the variation we are interested in, but it is possible that some real features could be suppressed.

The pre-anthropogenic background level assumed in our inversions influences the emissions estimated for the early part of the calculation, and we include uncertainty in the background level in our uncertainty calculation, using conservative ranges of 33.66–34.82 ppt for CF_4, 0.0–0.01 ppt for C_2F_6 and 0.0–0.001 ppt for C_3F_8. In Fig. 5c, CF_4 emissions are calculated by InvE2 using different values of the background level. For the low background levels, the inversion includes some emissions in the early 1900s, and for the high levels the increase of emissions from zero is around 5 years later than with the other values. The model–data mismatch is lowest for the CF_4 background level of 34.05 ppt (using the UEA to SIO calibration scale conversion equation given in Appendix A).

The results shown by the lines in Figs. 2, 3 and 4 are our preferred solutions calculated with Green's functions from the CSIRO model, and the confidence intervals use the ensemble of Green's functions from both firn models.

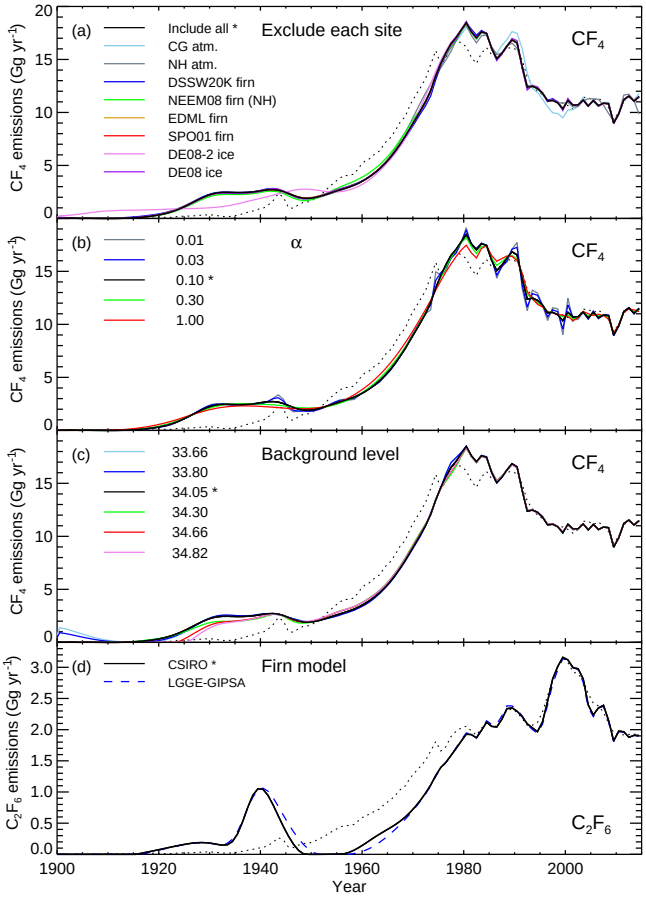

Figure 5. **(a)** CF_4 emissions estimated by InvE2 with measurements from all sites (black) and with each site excluded one at a time. **(b)** CF_4 emissions estimated using alternative values of the regularisation parameter α. **(c)** CF_4 emissions estimated using alternative values of the pre-anthropogenic background level. **(d)** C_2F_6 emissions inferred with the preferred Green's functions from the CSIRO (black solid line) and LGGE-GIPSA (blue dashed line) firn models. In all panels, our standard case is indicated in the legend by an asterisk, and the prior emissions are shown by the dotted lines.

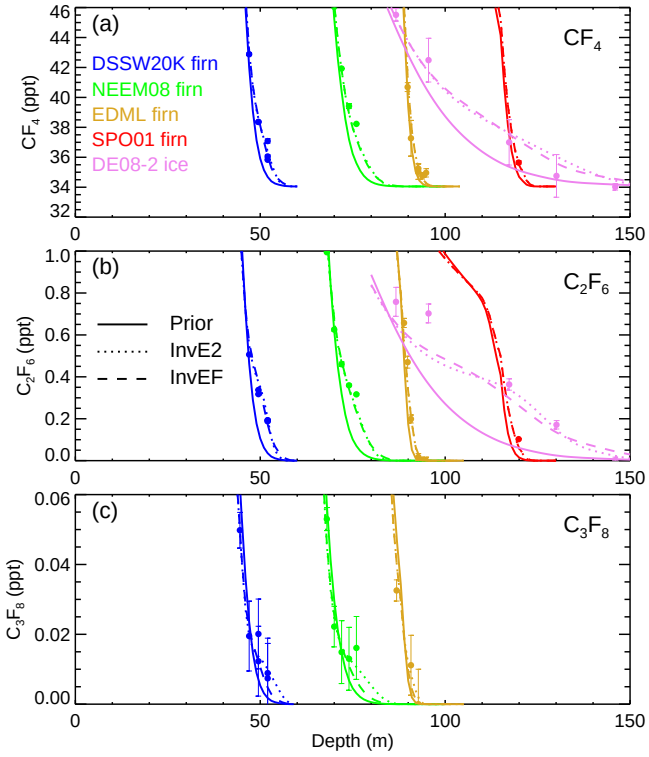

Figure 6. Mole fraction depth profiles at the bottom of the firn and in the DE08-2 ice for **(a)** CF_4, **(b)** C_2F_6 and **(c)** C_3F_8. Solid lines show mole fraction depth profiles for the prior, dotted lines are InvE2 emissions and dashed lines are for InvEF emission factor. Symbols show measurements with 1σ uncertainties.

In Fig. 5d we compare C_2F_6 emissions calculated with the InvE2 inversion using the preferred Green's functions from the CSIRO firn model (black line) with emissions calculated using the preferred Green's functions from the LGGE-GIPSA firn model (blue dash-dotted line). The difference between emissions inferred with Green's functions from the CSIRO and LGGE-GIPSA firn models is most noticeable for C_2F_6 but still fairly small for all three PFCs.

3.4 Deep firn and ice

Figure 6 shows the mole fraction depth profiles in the deep firn and ice, for the prior and InvE2 and InvEF inversions. They highlight how much the differences in emissions for the three cases make to the mole fraction depth profiles and therefore give an indication of the size of the mismatch in the mole fraction profile that we are interpreting in terms of emissions or emission factor. The mole fraction near the bottom of the firn contains information about the timing and the rate of increase in atmospheric mole fraction from zero, although interpretation is subject to uncertainties in the firn model. DE08 is not shown because all measurements are at pre-anthropogenic background levels.

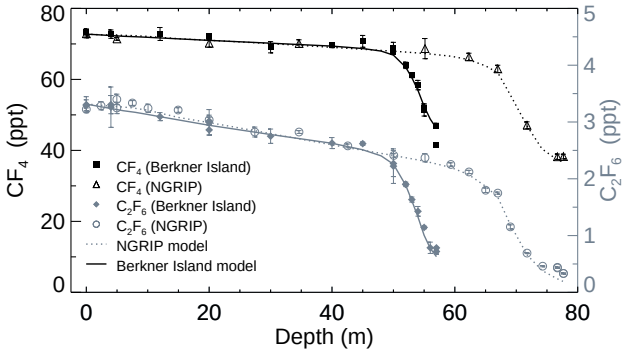

Figure 7. CF_4 and C_2F_6 at Berkner Island and North GRIP. Symbols show measurements from Worton et al. (2007), which were not used in our inversions. Lines show modelled depth profiles created by convolving our inferred atmospheric mole fraction time series in the appropriate hemisphere with Green's functions from the LGGE-GIPSA firn model. CF_4 is shown in black (left axis) and C_2F_6 in grey (right axis).

The difference between the prior and estimated mole fraction depth profiles, relative to the data uncertainty, is most obvious for C_2F_6 but is quite consistent for all of the firn sites as well as DE08-2. Inversions InvE2 and InvEF both lead to fairly similar depth profiles, indicating that it would not be worth trying to distinguish between the temporal variation of these two solutions (in particular, the timing and magnitude of the peaks in CF_4 and C_2F_6 emissions around 1940). This also implies that it is not worthwhile to reduce the value of α that scales the year-to-year constraint in the inversion in order to try to extract more information about the shorter-timescale variation from the firn data by allowing solutions with greater temporal variability, because the firn data are unlikely to constrain such variation.

3.5 Comparison with additional firn measurements

Worton et al. (2007) measured CF_4 and C_2F_6 in firn at Berkner Island, Antarctica, and NGRIP, Greenland, and inferred atmospheric histories from 1955 (for CF_4) and 1940 (for C_2F_6). We did not use these measurements in our inversions; instead we saved them for validation. In Fig. 7 we compare the Berkner Island and NGRIP measurements with our preferred mole fraction time series inferred by InvE2 convolved with Green's functions from the LGGE-GIPSA firn model. We have converted the Worton et al. (2007) firn measurements from the UEA calibration scale to the SIO calibration scale using the equations in Appendix A. We find very good agreement between our modelled depth profiles and the Berkner Island and NGRIP firn measurements from Worton et al. (2007).

A particular strength of this work comes from the fact that the inferred histories of emissions give a good match to overlapping atmospheric, firn and ice core measurements from eight different firn and ice core sites with very different cli-

mate and snow accumulation characteristics, collected at different times, with measurements made at two different laboratories and interpreted using two different firn models. This gives us increased confidence that the firn and ice core data provide a consistent and reliable picture of 19th and 20th century greenhouse gas changes.

4 Discussion

4.1 Pre-anthropogenic levels

Our oldest samples are from DE08 and contain air with CF_4 and C_2F_6 mean ages of 1841 and 1837, respectively, and Green's functions extending to before 1810. The oldest EDML firn sample also has PFC Green's functions extending back to before 1810. Our early measurements therefore tell us about PFCs from about 1800. The measured mole fractions of C_2F_6 and C_3F_8 were below the detection limits of 0.002 and 0.01 ppt, respectively, in the deepest EDML firn samples and several ice core samples (C_2F_6 only), indicating that 19th century levels of both C_2F_6 and C_3F_8 were either zero or extremely small. The oldest samples were all measured at UEA, as all of the samples measured on the Medusa systems contained at least some air from the 1940s or later. Mühle et al. (2010) estimated a C_2F_6 pre-industrial level of 0.1 ± 0.02, based on firn air from the Megadunes site in Antarctica with a mean age of about 1910, but no account was taken of the age distribution of that sample. It is quite likely that it contained some air from the 1940s or later, which explains the non-zero C_2F_6 measurement. For example, our South Pole firn sample at 120 m has a C_2F_6 mean age of about 1903 but measured mole fraction of about 0.1 ppt because the age distribution (red curve in Fig. 3b) includes some air from the 1940s and possibly 1950s. This highlights the need to consider the age distribution for interpretation of firn and ice core measurements, rather than characterising the age with a single number.

The DE08 ice core measurements of CF_4 (purple symbols in Fig. 2a) are constant with depth, indicating that CF_4 levels in the 19th century were stable. The low measurement must be an outlier rather than reflecting real atmospheric variations, due to the long lifetime of CF_4 and the fact that the Green's functions of nearby measurements have significant overlap. For CF_4, our oldest samples come from measurements made at UEA, so the conversion of measurements from the UEA calibration scale to the SIO-05 calibration scale is important for determining the pre-anthropogenic CF_4 level in the SIO-05 calibration scale. Using our best estimate for the factors relating the UEA to SIO-05 calibration scales (Appendix A), we estimate that CF_4 was stable at 34.1 ± 0.3 ppt during the 19th century, before anthropogenic influence became significant (after about 1910). The uncertainty is 1σ and takes into account measurement uncertainty and uncertainty in the UEA vs. SIO calibration scale. This uncertainty does not include the uncertainty in the CF_4 primary calibration scale, which is 1–2 % (Mühle et al., 2010).

Mühle et al. (2010) estimated a CF_4 pre-industrial background level of 34.7 ± 0.2, higher than our estimate, based on ice core measurements from Pâkitsoq, Greenland, and a Megadunes firn sample. The Megadunes firn measurement of 34.90 ± 0.04 ppt is likely to be higher than the background level because the sample probably contains some air from the 1940s or later (as for C_2F_6 described above). Pâkitsoq ice samples correspond to air with ages ranging between 19 000 and 11 360 BP, and Mühle et al. (2010) reported an average CF_4 mole fraction of 34.66 ± 0.16 ppt for these measurements. However, these samples have not been corrected for the effect of gravitational settling in firn. After correcting for gravitational effects using measured $\delta^{15}N_2$ (Schaefer et al., 2009, Jeff Severinghaus and Vas Petrenko, personal communication, 2016), the average of the Pâkitsoq ice samples is 33.75 ± 0.2 ppt. This is slightly lower than our estimate of 34.05 ± 0.33 ppt for the 19th century, but the difference is small considering the uncertainties in each estimate. The period from 11 360 to 19 000 covers the last deglaciation and back into the last glacial. It is possible that atmospheric CF_4 may have varied to some extent since then. Schmitt et al. (2013) found variations in CF_4 ranging between about 31 and 35 ppt over the last 800 000 years, with increasing CF_4 mole fraction during interglacials and decreasing CF_4 during glacials, which they attributed to variations in weathering due to climate, although tectonic activity is likely to be important too (Deeds et al., 2015).

The natural CF_4 source (due to rocks) is very small (of order $0.01\ \mathrm{Gg\,yr^{-1}} = 10\ \mathrm{t\,yr^{-1}}$ to maintain a background level of 34 ppt with an atmospheric lifetime of 50 000 years). The natural source is very much smaller than anthropogenic emissions and unlikely to have caused significant variations in atmospheric CF_4 in the last few hundred years.

4.2 Emissions peaks during World War II

Inversions InvE2 and InvEF for CF_4 and C_2F_6 both show a significant peak in emissions around 1940 (Figs. 2d and 3d), most likely associated with increased aluminium production during World War II (Barber and Tabereaux, 2014), for example for construction of aircraft. The peak is more prominent in C_2F_6 than CF_4. We expect to see a small peak after 1940 in inversion InvEF, because emissions are calculated as inferred EF multiplied by global aluminium production, and the aluminium production estimates (U.S. Geological Survey, 2014) contain a peak in the 1940s (Fig. 2e). However, the magnitude of the emissions peak from InvEF for both CF_4 and C_2F_6 is higher than we had expected (based on the prior estimate with constant emission factor) and comes from the high emission factor that the inversion requires to match the measurements. The peaks in InvE2, in contrast, come from the firn and ice core measurements and occur even if we remove the peak from the prior estimate. The peak in CF_4

is spread from about 1930 to 1945, but the peak in C_2F_6 is more prominent and of shorter duration. The DE08-2 ice core measurements have the narrowest age spread of the sites we consider (and possibly of any other firn or ice core sites that have been sampled to date) and are the ones that contain most information on this peak (Sect. 3.4). The peaks are about at the limit of what we can expect to resolve from firn and ice core measurements. We have no ice core measurements of C_3F_8, and the mole fraction level around 1940 is so low that if a similar peak existed in C_3F_8 it may be difficult to detect.

4.3 Emissions factors

Emission factors for PFC emissions from aluminium production have decreased markedly since the early 20th century, from around 2.1–4.4 kg t^{-1} for CF_4, 0.49–0.72 kg t^{-1} for C_2F_6 and 0.004–0.05 kg t^{-1} for C_3F_8 in 1940 (ranges are 95 % confidence intervals) to about 0.04, 0.003 and 0.0001 kg t^{-1} in recent years (Fraser et al., 2013). Our high estimates of emission factors in the early 20th century are plausible. In the early days of aluminium production, there was little alumina feeding control (Edwards et al., 1930), which would undoubtedly have resulted in very frequent anode effects and therefore high PFC emission rates. Averaged across more than 10 USA smelters in 1990 there were 3 anode effect minutes per cell per day, obtained by multiplying the anode effect frequency (per cell day) by the anode effect duration (minutes) (personal communication, Alton Tabereaux, Alcoa). Before the 1950s, there could have been 9–15 anode effect mins/cell/day, which is 3–5 times higher than in 1990. If we assume that the average 1990 CF_4 emission factor was 1.2 kg t^{-1}, then a pre-1950s emission factor could have been 3.6–6.0 kg t^{-1}, which is about what we see in our inversion. After the 1950s, there was more awareness of the extra costs associated with anode effects due to loss in metal production and extra energy consumption. Thus plants developed more sophisticated alumina feed control systems, leading to reduced frequency of anode effects.

4.4 Latitudinal distribution of emissions

The InvE1 inversion gives estimates of monthly semi-hemispheric emissions. Although the estimates of the north–south distribution of emissions are sensitive to uncertainties in model transport parameters, we can draw some general conclusions about shifts in the distribution over time. Between 1980 and 2010, we see an increase of the proportion of global CF_4 emissions in the 0–30° N and 0–30° S boxes, with a corresponding decrease in the proportion of global emissions in the 30–90° N box (roughly 20 % of the total emissions). Over this period, we also see an increase in the proportion of global C_2F_6 emissions in 0–30° N box, along with a decrease in the 30–90° N box (also about 20 % of the total). There is no clear change in the latitudinal distribution of C_3F_8 emissions. We note that our inversion using the AGAGE 12-box model is not particularly well suited to this type of conclusion, and analysis with a model that has more accurate atmospheric transport, such as a 3-D atmospheric transport model, would be required to obtain a robust result. However, a general equatorward shift of a proportion of the emissions is consistent with the rapid rise of China into the aluminium market from the 1990s into the 2000s (International Aluminium Institute, 2009, 2014) at a lower latitude on average than previous emissions based in North America and Europe, for example in locations such as Canada and Norway (a map of the location of many aluminium smelters is shown in Wong et al. (2015), with a significant number of Chinese smelters south of 30° N). The emergence of semiconductor emissions in recent decades, with significant contributions of emissions from Asia, would also have caused an equatorward shift of a proportion of the emissions.

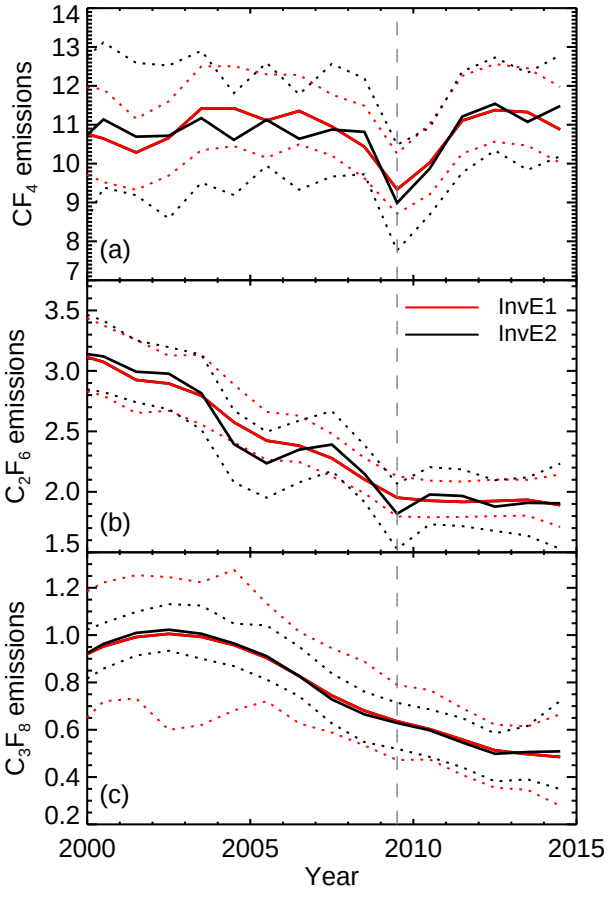

Figure 8. (a) CF_4, **(b)** C_2F_6 and **(c)** C_3F_8 emissions (Gg yr^{-1}) from 2000 for the InvE1 inversion in red and the InvE2 inversion in black. Uncertainty ranges shown for both models are 95 % confidence intervals.

4.5 Global financial crisis (GFC)

Our study adds an extra 6 years of measurements compared to Mühle et al. (2010), extending the estimated emissions

to the end of 2014. Figure 8 shows the estimated emissions from both the InvE1 and InvE2 inversions for the three PFCs from 2000. Our best estimates for CF_4 emissions from both inversions varied mostly within the range $11 \pm 0.5\,\mathrm{Gg\,yr^{-1}}$ between 1998 and 2007, before dropping by about 15 % in 2009, presumably due to reduced economic activity associated with the GFC. CF_4 emissions in 2010 recovered some of this drop, then from 2011 to 2014 they varied about a mean level that was slightly higher than the 1998–2007 mean. The prior estimate for emissions growth rate used by the InvE1 inversion for CF_4 was constant (i.e. assumes no emissions growth) from 2008, so the inferred dip must be due to the atmospheric observations. Emissions of C_2F_6 from the InvE2 inversion also show a dip in 2009, in addition to the already decreasing trend between 1998 and 2007. The InvE1 inversion does not show a clear C_2F_6 dip. C_2F_6 emissions in both inversions were fairly steady from 2010. C_3F_8 emissions peaked about 2002, then decreased until 2012 and have been steady since. They do not seem to show an additional reduction around 2009 above the already decreasing trend, but both inversions have little interannual variability in their inferred emissions. The magnitude of the dip in the inferred emissions will be sensitive to the statistics of each inversion including data uncertainties and regularisation, although we see that the CF_4 dip barely changes with the choice of the regularisation parameter α in Fig. 5b. The growth rate of a trend curve with 650 day smoothing fitted to Mace Head monthly PFC mole fraction shows pronounced dips in 2009 in CF_4 and C_3F_8 but only a small dip in C_2F_6.

Global emissions of CO_2 show a dip in 2009 due to the GFC (Friedlingstein et al., 2010), followed by a rapid recovery (Peters et al., 2012), although the dip was only around 1.4 % and was dominated by emissions in developed countries and offset by increases in emissions in developing countries. Estimates of global primary aluminium production from the International Aluminium Industry show a 6 % reduction in 2009 compared to 2008, dominated by developed countries but with steady levels from China. The price of primary aluminium dropped by more than half from 2008 to 2009 (Barber and Tabereaux, 2014). Kim et al. (2014) (also shown in Wong et al., 2015) showed global top-down and bottom-up emissions estimated to 2010, and they have dips at the time of the GFC in the top-down estimates as well as both the aluminium and semiconductor components of the bottom-up emissions, but they were not specifically discussed nor related to the GFC. The 2009 dip in bottom-up CF_4 emissions given by Kim et al. (2014) is 23 % for both aluminium and semiconductor emissions and 24 and 26 % in bottom-up aluminium and semiconductor C_2F_6 emissions, respectively.

4.6 Recent years

While the initial reduction of PFC emission factors last century was a consequence of measures to reduce electricity consumption during aluminium production, in recent decades there has been a concerted effort by both the aluminium and semiconductor industries to reduce PFC emissions. However, the rate of decrease of emissions appears to have slowed and possibly stopped in recent years. Other than the 2009 dip, CF_4 emissions have been quite steady since about 1998, C_2F_6 emissions have been steady since about 2010 and the decline in C_3F_8 emissions appears to have recently stopped. Primary aluminium production has increased year after year and at a greater rate from the year 2000, so steady emissions imply decreasing emission factors. However, due to the very long lifetimes of these gases, PFCs emitted become effectively a permanent part of the atmosphere and therefore make an enduring contribution to radiative forcing. The long lifetimes, together with their exceptionally high global warming potentials, underpin the urgent need for continued reduction of PFC emissions from all PFC generating industries. This should involve further mitigation efforts by the two major emitting industries (aluminium and semiconductors) and better quantification of emissions and (if necessary) mitigation efforts for the other potential sources (e.g. HCFC/fluorochemical production and rare earth industries).

5 Summary and conclusions

We have reconstructed emissions and atmospheric abundance of CF_4, C_2F_6 and C_3F_8 from 19th century levels (prior to anthropogenic influence) to 2014, using measurements from four firn sites, two ice cores and archived and in situ atmospheric air from both hemispheres. We also inferred emission factors for PFC emissions due to aluminium production prior to the 1980s. These are the first continuous records of PFC mole fraction and emissions from pre-anthropogenic to recent times. They demonstrate how unintended consequences of human actions and deliberate mitigation efforts have affected these important atmospheric constituents over the past century.

The 19th century levels of CF_4 were stable at 34.1 ± 0.3 ppt and below detection limits of 0.002 and 0.01 ppt for C_2F_6 and C_3F_8. CF_4 and C_2F_6 both show peaks in emissions around 1940, presumably due to increased demand for aluminium production during World War II. These peaks are about at the limit of the time resolution recoverable from ice core and firn measurements. We estimate emission factors in 1940 of 2.2–4.8 $\mathrm{kg\,t^{-1}}$ for CF_4, 0.38–0.53 $\mathrm{kg\,t^{-1}}$ for C_2F_6 and 0.003–0.04 $\mathrm{kg\,t^{-1}}$ for C_3F_8.

At the recent end of the record, we see temporary reductions in CF_4 (and perhaps C_2F_6) emissions in 2009, presumably associated with the impact of the GFC on global alu-

minium and semiconductor production. The strong decrease in PFC emissions that we have seen since the peaks in 1980 (CF_4) and early-to-mid-2000s (C_2F_6 and C_3F_8) appears to have slowed and possibly stopped in recent years. Continued effort from *all* PFC generating industries is urgently needed to reduce the emissions of these potent greenhouse gases, which, once emitted, will stay in the atmosphere essentially permanently (on human timescales) and contribute to radiative forcing.

6 Data availability

The firn, ice core and archive PFC measurements and the reconstructed histories of mole fraction, emissions and emission factor are available in the Supplement. The in situ measurements are available on the CDIAC website doi:10.3334/CDIAC/atg.db1001.

Appendix A: SIO and UEA calibration scales

The present study combines firn and in situ PFC measurements made on the Medusa system (reported on the SIO calibration scale) with firn and ice core measurements from DE08, DE08-2 and EDML made only at the University of East Anglia (reported on the UEA calibration scale). To combine these data we need to ensure that they are on the same calibration scale, so we convert the UEA measurements to the SIO calibration scale (SIO-05 for CF_4 and SIO-07 for C_2F_6 and C_3F_8). We have some firn PFC measurements made on the Medusa system and at UEA at common sites and depths; in some cases the samples measured at one laboratory were subsamples of those measured at the other, and in other cases they were separate samples taken from the same firn sites and depths. For CF_4 we have corresponding samples from DSSW20K, DSSW19K and SPO 2001, for C_2F_6 we have DSSW20K, DSSW19K, SPO 2001 and NEEM 2008 and for C_3F_8 we have only NEEM 2008. DSSW19K is a firn site about 1 km from DSSW20K on Law Dome that was sampled in October 2004 in 35 L stainless steel tanks that were filled with undried air via the firn air sampling device to pressures of about 4 bar. There was suspected contamination of some of the DSSW19K samples during collection, so they have not been used for the reconstruction of PFCs, but the same samples were measured on both the Medusa and UEA systems, making them valuable for calibration scale comparison over our range of interest.

Figure A1a–c show measurements on the UEA calibration scale plotted against measurements made on the Medusa at the same firn depths. Figure A1d–f show the same data but plotted as the difference in percent vs. the Medusa measurements, to show nonlinear differences in calibration scale if they exist. The Medusa measurements of CF_4 and C_2F_6 were made at three different times (several years apart) by different people, and these are shown separately, with separate linear least-squares fits. The NEEM 2008 Medusa measurements of C_3F_8 were only made once, and we show some additional measurements (open circles) made at similar depths (mostly different by about 0.05 m but up to 0.25 m). The difference in percent for CF_4 and C_2F_6 is quite consistent, except for scatter of C_2F_6 at low mole fraction (below about 0.4 ppt). The C_3F_8 measurements show some nonlinearity at very low mole fraction (below about 0.03 ppt), but these are below the detection limit.

The linear least-squares fit to all CF_4 measurements in Fig. A1a is shown by the red dashed line, and we use this to convert the UEA firn measurements to the SIO-05 calibration scale as follows:

$$[CF_4]_{\text{SIO-05}} = \frac{[CF_4]_{\text{UEA}} + 0.117}{1.0643}.$$

The range given by the four different linear fits shown in Fig. A1a, as well as a linear fit that is forced through the origin $[CF_4]_{\text{SIO-05}} = [CF_4]_{\text{UEA}}/1.0621$, is incorporated into the data uncertainties for the UEA measurements, to reflect uncertainty in the calibration scale conversion.

The fit to all C_2F_6 measurements gives

$$[C_2F_6]_{\text{SIO-07}} = \frac{[C_2F_6]_{\text{UEA}} - 0.0270}{0.849},$$

(shown by the red dashed line) which we use to convert the UEA measurements. Some UEA C_2F_6 measurements with zero mole fraction in the UEA calibration scale would end up negative; these are set to zero. The intercept in the data fits is around the detection limit and of the order of the uncertainty in the measurements. Data uncertainties assigned to the UEA measurements incorporate the spread from the different linear fits, including one through the origin.

We have only one set of measurements for C_3F_8, giving

$$[C_3F_8]_{\text{SIO-07}} = \frac{[C_3F_8]_{\text{UEA}} + 0.001}{0.949}.$$

The measurements at similar depths were not used to determine the fit, just to give more points for comparison. A linear fit to the NEEM 2008 C_3F_8 passing through the origin is

$$[C_3F_8]_{\text{SIO-07}} = \frac{[C_3F_8]_{\text{UEA}}}{0.946}.$$

Appendix B: Measurement details

Air was extracted from DE08 and DE08-2 ice core sections at CSIRO using a "cheese grater" dry extraction system (Etheridge et al., 1988, 1996; Rubino et al., 2013). Ice sections were approximately 800 g in weight and grated after evacuation in a cold room at −20 °C with the extraction vessel and ice having been pre-chilled to −80 °C. The air released by grating from the bubbles in the ice were recollected by cryogenically pumping through an ice–ethanol mixture at −100 °C (to remove water vapour) into a stainless steel cold finger held at < 18 K on the cold stage of a helium compressor cryostat. On warming to room temperature these cold fingers acquired an internal pressure of several atmospheres. These were then shipped to UEA for analysis. Several tests were made extracting bubble-free ice (as a blank), and transferring firn air of known PFC content into the cold fingers (with and without bubble-free ice) to determine system blank levels and to ensure that PFC abundance was unaffected by the ice extraction and air transfer and trapping process.

At UEA the PFCs from EDML firn air and air released from the ice cores were analysed using a high-sensitivity gas chromatograph/trisector mass spectrometer system (Waters/Micromass Autospec) according to the procedures detailed in Worton et al. (2007) and Mani (2010). The volumes of firn air measured were limited to 100 cm^{-3} to avoid breakthrough of the cryogenic preconcentration system, whilst volumes of between ca. 10 and 50 cm^{-3} were analysed from

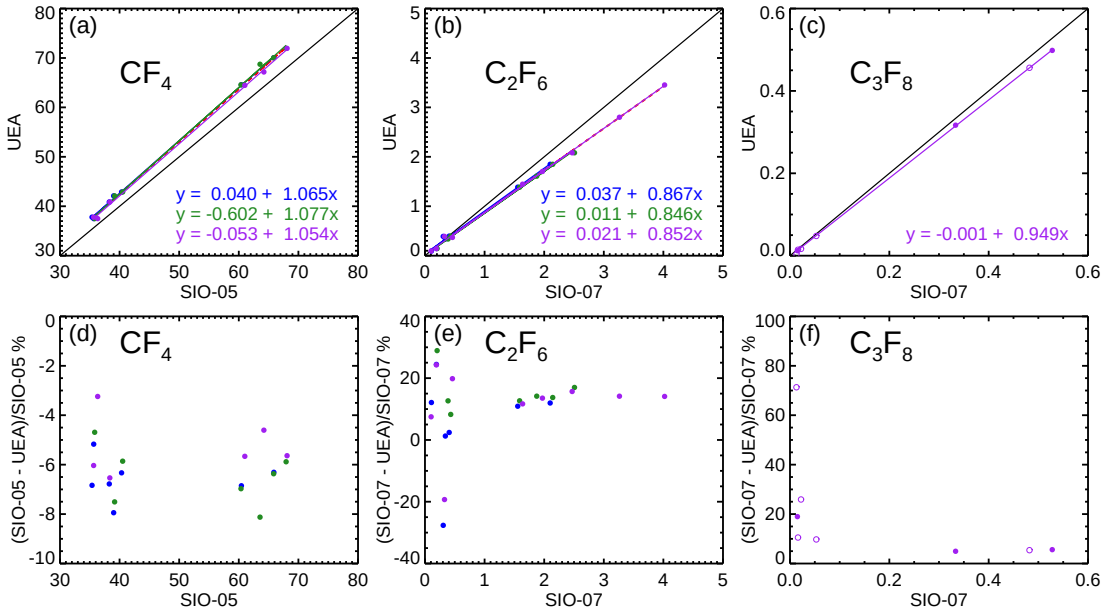

Figure A1. (a) Circles show measurements of CF_4 made at UEA plotted against measurements at the same firn depths measured at Aspendale or Cape Grim on the Medusa system, for firn sites DSSW20K, DSSW19K and SPO 2001. The Medusa measurements were made at three separate times by different people, and these are plotted in different colours. Linear fits to these data are shown with their equations. The red dashed line shows the fit to all measurements, given in the main text. The black line shows the 1 : 1 line. **(b)** As in **(a)** but for C_2F_6 with measurements from DSSW20K, DSSW19K, SPO 2001 and NEEM 2008. **(c)** Medusa measurements of C_3F_8 at NEEM 2008 plotted against UEA measurements. The filled circles show measurements at the same depths (these data were used to determine the linear fit), while the open circles show measurements at similar depths. **(d–f)** Same data as in **(a–c)** but plotted as a percent difference.

the ice core cold fingers. Volumetric linearity tests were performed. Calibration procedures are discussed in Worton et al. (2007).

Analysis of firn air on the Medusa system was described in Vollmer et al. (2016).

Appendix C: Firn model diffusivity calibration

EDML is located near Kohnen Station, Dronning Maud Land, Antarctica (Weiler, 2008; Mani, 2010). Firn air was collected in January 2006. We model EDML with an accumulation rate of 65 kg m^{-2} yr^{-1}, temperature of 228 K and pressure of 730 mb. The density profile used in the firn models is based on measurements given in Weiler (2008). Diffusivity in the CSIRO firn model was calibrated for EDML using measurements of CO_2, SF_6, CFC-12, CFC-113, CFC-115, HCFC-142b, HFC-23 and $\delta^{15}N_2$, as shown in Supplement Fig. S1. Diffusivity in the LGGE-GIPSA firn model was tuned for EDML using measurements of CO_2, SF_6, CFC-12 and CFC-113, with the method, atmospheric reconstructions and diffusion coefficients described in Witrant et al. (2012) (Supplement Fig. S2).

The LGGE-GIPSA firn model was tuned for DSSW20K using measurements of CO_2, CH_4, SF_6, CFC-11, CFC-12, CFC-113, CH_3CCl_3, HFC-134a, $^{14}CO_2$ and HCFC-141b. Three diffusivity solutions for the LGGE-GIPSA model are shown in Supplement Fig. S3. The dashed blue and red lines show diffusivity calibrated with the method of Witrant et al. (2012) for two different atmospheric CO_2 reconstructions. The black line shows diffusivity calibrated using the same calibration method but with some model inputs (density, closed porosity and data uncertainties) that were used in the CSIRO firn model.

Appendix D: Annual mole fraction data from in situ and archive measurements

To obtain annual mole fraction data for the high northern and southern latitudes, we fit smoothing splines to measurements from Cape Grim (air archive and in situ) and Mace Head (in situ) and the suite of old tanks from the Northern Hemisphere. The splines are sampled at 1-year intervals to give mole fraction corresponding to the start of each year. For the period covered by the air archives, where there are not reliable measurements in every year, we only retain annual values when there are air archive measurements around the same time. The splines have 50 % attenuation at periods of 1 year. Figure D1 shows the original measurements and annual mole fraction data.

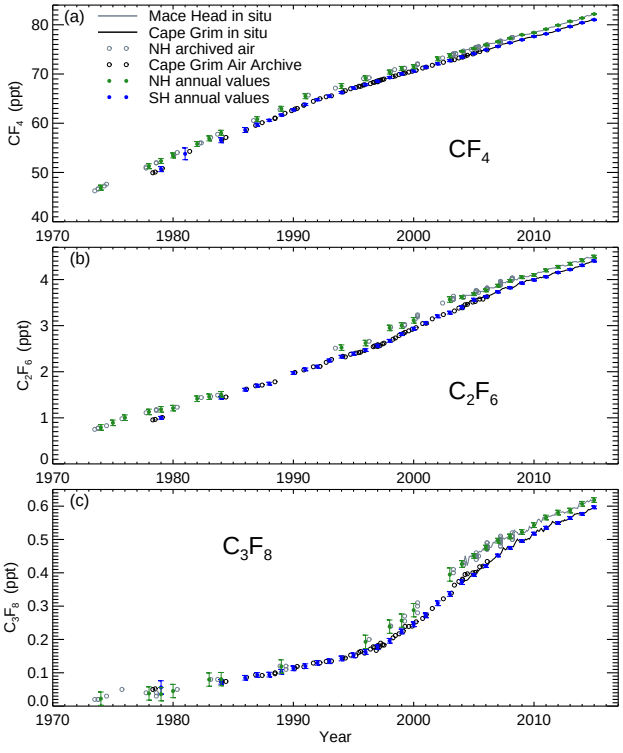

Figure D1. **(a)** Mace Head and Cape Grim in situ monthly CF_4 are shown by the solid lines. Cape Grim air archive and northern hemispheric air archive measurements are the open circles. Blue and green circles show selected northern hemispheric (NH) and southern hemispheric (SH) annual values from a spline fit to the observations that has 50 % attenuation at periods of 1 year. Error bars show 1σ uncertainties assigned to the annual means and used in the synthesis inversion. **(b)** Same for C_2F_6. **(c)** Same for C_3F_8.

The Supplement related to this article is available online at doi:10.5194/acp-16-11733-2016-supplement.

Author contributions. C. M. Trudinger, P. J. Fraser, D. M. Etheridge and W. T. Sturges designed the study; M. K. Vollmer, D. R. Worton, B. R. Miller, J. Laube and F. Mani performed PFC measurements on firn or ice core samples; P. J. Fraser, W. T. Sturges, J. Mühle, P. B. Krummel, L. P. Steele, C. M. Harth and S. O'Doherty contributed to the in situ records and general PFC measurement capability; D. M. Etheridge, T. Blunier, J. Schwander and M. Battle collected ice or firn air; C. M. Trudinger developed and ran the CSIRO firn model and InvE2 and InvEF inversions; M. Rigby developed and ran the InvE1 inversions; P. Martinerie and E. Witrant developed and ran the LGGE-GIPSA firn model; P. J. Rayner contributed ideas on modelling and uncertainties; C. M. Trudinger wrote the paper with input from other authors.

Acknowledgements. This work has been undertaken as part of the Australian Climate Change Science Program, funded jointly by the Department of the Environment, the Bureau of Meteorology and CSIRO. We acknowledge support from the Australian Antarctic Science Program. This work is a contribution to the European Project for Ice Coring in Antarctica (EPICA), a joint European Science Foundation/European Commission scientific programme, funded by the European Union (EPICA-MIS) and by national contributions from Belgium, Denmark, France, Germany, Italy, the Netherlands, Norway, Sweden, Switzerland and the United Kingdom. This work was also funded by the CEC programme (EUK2-CT2001-00116, CRYOSTAT). NEEM is directed and organised by the Center of Ice and Climate at the Niels Bohr Institute and US NSF, Office of Polar Programs, and is supported by funding agencies and institutions in Belgium (FNRS-CFB and FWO), Canada (NRCan/GSC), China (CAS), Denmark (FIST), France (IPEV, CNRS/INSU, CEA and ANR), Germany (AWI), Iceland (RannIs), Japan (NIPR), Korea (KOPRI), the Netherlands (NWO/ALW), Sweden (VR), Switzerland (SNF), United Kingdom (NERC) and the USA (US NSF, Office of Polar Programs). We acknowledge the support of the CSIRO GASLAB team. The operation of the AGAGE instruments at Mace Head and Cape Grim is supported by the National Aeronautic and Space Administration (NASA) (grants NAG5-12669 and NNX07AE89G to MIT; grants NNX07AF09G and NNX07AE87G to SIO), the Department of Energy and Climate Change (DECC, UK) contract GA01081 to the University of Bristol, CSIRO and Bureau of Meteorology (Australia). William Sturges recognises the CSIRO Fröhlich Fellowship for supporting a visit to CSIRO Aspendale. Martin Vollmer acknowledges a CSIRO Office of the Chief Executive Distinguished Visiting Scientist grant to CSIRO Aspendale for firn air measurements. Matthew Rigby is supported by an advanced research fellowship (NE/I021365/1) from the UK Natural Environment Research Council (NERC). Francis Mani was supported by a Marie Curie Fellowships in Antarctic Air-Sea-Ice Science award, David Worton by a NERC Studentship, and Johannes Laube by a NERC Fellowship (NE/I021918/1). We thank Cecelia MacFarling-Meure for ice extraction, Jean-Marc Barnola, Andrew Smith, Tas van Ommen, Dominic Ferretti and Mark Curran for helping to collect the Law Dome firn and ice samples and Pep Canadell and Roger Francey for helpful comments on the manuscript.

Edited by: A. Jones
Reviewed by: two anonymous referees

References

Aydin, M., Saltzman, E. S., De Bruyn, W. J., Montzka, S. A., Butler, J. H., and Battle, M.: Atmospheric variability of methyl chloride during the last 300 years from an Antarctic ice core and firn air, Geophys. Res. Lett., 31, L02109, doi:10.1029/2003GL018 750, 2004.

Barber, M. and Tabereaux, A. T.: The Evolution of Soderberg Aluminum Cell Technology in North and South America, JOM, 66, 223–234, doi:10.1007/s11837-013-0855-1, 2014.

Buizert, C., Martinerie, P., Petrenko, V. V., Severinghaus, J. P., Trudinger, C. M., Witrant, E., Rosen, J. L., Orsi, A. J., Rubino, M., Etheridge, D. M., Steele, L. P., Hogan, C., Laube, J. C., Sturges, W. T., Levchenko, V. A., Smith, A. M., Levin, I., Conway, T. J., Dlugokencky, E. J., Lang, P. M., Kawamura, K., Jenk, T. M., White, J. W. C., Sowers, T., Schwander, J., and Blunier, T.: Gas transport in firn: multiple-tracer characterisation and model intercomparison for NEEM, Northern Greenland, Atmos. Chem. Phys., 12, 4259–4277, doi:10.5194/acp-12-4259-2012, 2012.

Butler, J. H., Montzka, S. A., Battle, M., Clarke, A. D., Mondeel, D. J., Lind, J. A., Hall, B. D., and Elkins, J. W.: Collection and Analysis of Firn Air from the South Pole, 2001, AGU Fall Meeting Abstracts, p. F145, 2001.

Cicerone, R. J.: Atmospheric carbon tetrafluoride: A nearly inert gas, Science, 206, 59–61, 1979.

Cunnold, D. M., Fraser, P. J., Weiss, R. F., Prinn, R. G., Simmonds, P. G., Miller, B. R., Alyea, F. N., and Crawford, A. J.: Global Trends and Annual Releases of CCl_3F and CCl_2F_2 Estimated from ALE/GAGE and other Measurements from July 1978 to June 1991, J. Geophys. Res., 99, 1107–1126, 1994.

Deeds, D. A., Vollmer, M. K., Kulongoski, J. T., Miller, B. R., Mühle, J., Harth, C. M., Izbicki, J. A., Hilton, D. R., and Weiss, R. F.: Evidence for crustal degassing of CF_4 and SF_6 in Mojave Desert groundwaters, Geochim. Cosmochim. Ac., 72, 999–1013, 2008.

Deeds, D. A., Kulongoski, J. T., Mühle, J., and Weiss, R. F.: Tectonic activity as a significant source of crustal tetrafluoromethane emissions to the atmosphere: Observations in groundwaters along the San Andreas Fault, Earth Planet. Sci. Lett., 412, 163–172, 2015.

EDGAR: Emission Database for Global Atmospheric Research, release version 4.1, European Commission, Joint Research Centre (JRC)/Netherlands Environmental Assessment Agency (PBL), available at: http://edgar.jrc.ec.europa.eu (last access: April 2015), 2010.

Edwards, J. D., Frary, F. C., and Jeffries, Z.: The Aluminium Industry: Aluminium and its Production, 1st Edn., McGraw-Hill, 310–311, 1930.

Efron, B. and Tibshirani, R. J.: An Introduction to the Bootstrap, Chapman and Hall, New York, 1993.

Etheridge, D. M., Pearman, G. I., and de Silva, F.: Atmospheric trace-gas variations as revealed by air trapped in an ice core from Law Dome, Antarctica, Ann. Glaciol., 10, 28–33, 1988.

Etheridge, D. M., Steele, L. P., Langenfelds, R. L., Francey, R. J., Barnola, J. M., and Morgan, V. I.: Natural and anthropogenic changes in atmospheric CO_2 over the last 1000 years from air in Antarctic ice and firn, J. Geophys. Res., 101D, 4115–4128, 1996.

Etheridge, D. M., Steele, L. P., Francey, R. J., and Langenfelds, R. L.: Atmospheric methane between 1000 AD and present: evidence for anthropogenic emissions and climate variability, J. Geophys. Res., 103D, 15979–15993, 1998.

Fraser, P., Steele, P., and Cooksey, M.: PFC and Carbon Dioxide Emissions from an Australian Aluminium Smelter Using Time-Integrated Stack Sampling and GC-MS, GC-FID Analysis, John Wiley & Sons, Inc., 871–876, doi:10.1002/9781118663189.ch148, 2013.

Friedlingstein, P., Houghton, R. A., Marland, G., Hackler, J., Boden, T. A., Conway, T. J., Canadell, J. G., Ciais, M. R. R. P., and Le Quéré, C.: Update on CO_2 emissions, Nat. Geosci., 3, 811–812, doi:10.1038/ngeo1022, 2010.

Fuller, E. N., Schettler, P. D., and Giddings, J. C.: A new method for prediction of binary gas-phase diffusion coefficients, Ind. Eng. Chem., 58, 19–27, 1966.

Harnisch, J.: Atmospheric perfluorocarbons: Sources and concentrations, in: Non-CO_2 greenhouse gases: Scientific understanding, control and implementation, edited by: van Ham, J., Baede, A. P. M., Meyer, L. A., and Ybema, R., Kluwer Academic Publishers, 1999.

Harnisch, J. and Eisenhauer, A.: Natural CF_4 and SF_6 on earth, Geophys. Res. Lett., 25, 2401–2404, 1998.

Holiday, R. D. and Henry, J. L.: Anode polarization and fluorocarbon formation in aluminium reduction cells, Ind. Eng. Chem., 51, 1289–1292, doi:10.1021/ie50598a036, 1959.

Institute for Environmental Protection and Research: Chapter 4. Industrial processes [CRF Sector 2] in Italian Greenhouse Gas Inventory 1990–2011, National Inventory Report, available at: http://unfccc.int/national_reports/annex_i_ghg_inventories/national_inventories_submissions/items/7383.php (last access: May 2016), 2013.

International Aluminium Institute: Results from the 2008 Anode Effect Survey, Report on the Aluminium Industry's Global Perfluorocarbon Gases Emissions Reduction Programme, London: International Aluminium Institute, available at: http://www.world-aluminium.org/media/filer_public/2013/01/15/fl0000300.pdf (last access: May 2016), 2009.

International Aluminium Institute: Results from the 2012 Anode Effect Survey, Report on the Aluminium Industry's Global Perfluorocarbon Gases Emissions Reduction Programme, London: International Aluminium Institute, available at: http://www.world-aluminium.org/media/filer_public/2013/08/20/2012_anode_effect_survey_report.pdf (last access: May 2016), 2014.

IPCC: 2006 IPCC Guidelines for National Greenhouse Gas Inventories, Prepared by the National Greenhouse Gas Inventories Programme, chap. 4 Metal Inventory Emissions, Published: IGES, Japan, http://www.ipcc-nggip.iges.or.jp/public/2006gl/pdf/3_Volume3/V3_4_Ch4_Metal_Industry.pdf (last access: August 2016), 2006.

Jubb, A. M., McGillen, M. R., Portmann, R. W., Daniel, J. S., and Burkholder, J. B.: An atmospheric photochemical source of the persistent greenhouse gas CF_4, Geophys. Res. Lett., 42, 9505–9511, doi:10.1002/2015GL066193, 2015.

Khalil, M. A. K., Rassmussen, R. A., Culbertson, J. A., Prins, J. M., Grimsrud, E. P., and Shearer, M. J.: Atmospheric perfluorocarbons, Environ. Sci. Technol., 37, 4358, doi:10.1021/es030327a, 2003.

Kim, J., Fraser, P. J., Li, S., Mühle, J., Ganesan, A. L., Krummel, P. B., Steele, L. P., Park, P., Kim, S., Park, M., Arnold, T., Harth, C. M., Salameh, P. K., Prinn, R. G., Weiss, R. F., and Kim, K.: Quantifying aluminium and semiconductor industry perfluorocarbon emissions from atmospheric measurements, Geophys. Res. Lett., 41, 4787–4794, doi:10.1002/2014GL059783, 2014.

Langenfelds, R. L., Fraser, P. J., Francey, R. J., Steele, L. P., Porter, L. W., and Allison, C. E.: The Cape Grim air archive: The first seventeen years, 1978–1995, in: Baseline Atmospheric Program (Australia) 1994–95, edited by: Francey, R. J., Dick, A. L., and Derek, N., Bureau of Meteorology and CSIRO Division of Atmospheric Research, Melbourne, Australia, 53–70, 1996.

Laube, J. C., Hogan, C., Newland, M. J., Mani, F. S., Fraser, P. J., Brenninkmeijer, C. A. M., Martinerie, P., Oram, D. E., Röckmann, T., Schwander, J., Witrant, E., Mills, G. P., Reeves, C. E., and Sturges, W. T.: Distributions, long term trends and emissions of four perfluorocarbons in remote parts of the atmosphere and firn air, Atmos. Chem. Phys., 12, 4081–4090, doi:10.5194/acp-12-4081-2012, 2012.

Li, W., Chen, X., Yang, J., Hu, C., Liu, Y., Li, D., and Guo, H.: Latest Results from PFC Investigation in China, 617–622, doi:10.1002/9781118359259.ch105, 2012.

Mani, F. S.: Measurements of δ^{15}N of nitrogen gas and composition of trace gases in air from firn and ice cores, PhD thesis, University of East Anglia, 2010.

Martinerie, P., Nourtier-Mazauric, E., Barnola, J.-M., Sturges, W. T., Worton, D. R., Atlas, E., Gohar, L. K., Shine, K. P., and Brasseur, G. P.: Long-lived halocarbon trends and budgets from atmospheric chemistry modelling constrained with measurements in polar firn, Atmos. Chem. Phys., 9, 3911–3934, doi:10.5194/acp-9-3911-2009, 2009.

Matsunaga, N., Hori, M., and Nagashima, A.: Measurements of the mutual diffusion coefficients of carbon tetrafluoride and methyl bromide into air, nitrogen and oxygen, in: Proc. 26th Jpn. Symp. Therm. Props, vol. 26, 499–501, 2005.

Menke, W.: Geophysical Data Analysis: Discrete Inverse Theory, revised edition, Academic Press, San Diego, 1989.

Miller, B. R., Weiss, R. F., Salameh, P. K., Tanhua, T., Greally, B. R., Mühle, J., and Simmonds, P. G.: Medusa: A Sample Preconcentration and GC/MS Detector System for in Situ Measurements of Atmospheric Trace Halocarbons, Hydrocarbons, and Sulfur Compounds, Anal. Chem., 80, 1536–1545, doi:10.1021/ac702084k, 2008.

Morris, R. A., Miller, T. M., Viggiano, A. A., Paulson, J. F., Solomon, S., and Reid, G.: Effects of electron and ion reactions on atmospheric lifetimes of fully fluorinated compounds, J. Geophys. Res.-Atmos., 100, 1287–1294, doi:10.1029/94JD02399, 1995.

Mühle, J., Ganesan, A. L., Miller, B. R., Salameh, P. K., Harth, C. M., Greally, B. R., Rigby, M., Porter, L. W., Steele, L. P., Trudinger, C. M., Krummel, P. B., O'Doherty, S., Fraser, P. J.,

Simmonds, P. G., Prinn, R. G., and Weiss, R. F.: Perfluorocarbons in the global atmosphere: tetrafluoromethane, hexafluoroethane, and octafluoropropane, Atmos. Chem. Phys., 10, 5145–5164, doi:10.5194/acp–10–5145–2010, 2010.

Mulder, I., Huber, S. G., Krause, T., Zetzsch, C., Kotte, K., Dultz, S., and Schöler, H. F.: A new purge and trap headspace technique to analyze low volatile compounds from fluid inclusions of rocks and minerals, Chem. Geol., 358, 148–155, doi:10.1016/j.chemgeo.2013.09.003, 2013.

Myhre, G., Shindell, D., Bréon, F.-M., Collins, W., Fuglestvedt, J., Huang, J., Koch, D., Lamarque, J.-F., Lee, D., Mendoza, B., Nakajima, T., Robock, A., Stephens, G., Takemura, T., and Zhang, H.: Anthropogenic and Natural Radiative Forcing, in: Climate Change 2013: The Physical Science Basis. Contribution of Working Group I to the Fifth Assessment Report of the Intergovernmental Panel on Climate Change, edited by: Stocker, T. F., Qin, D., Plattner, G.-K., Tignor, M., Allen, S., Boschung, J., Nauels, A., Xia, Y., Bex, V., and Midgley, P., Cambridge University Press, Cambridge, United Kingdom and New York, NY, USA, 733 pp., 2013.

Oram, D. E., Mani, F. S., Laube, J. C., Newland, M. J., Reeves, C. E., Sturges, W. T., Penkett, S. A., Brenninkmeijer, C. A. M., Röckmann, T., and Fraser, P. J.: Long-term tropospheric trend of octafluorocyclobutane (c-C4F8 or PFC-318), Atmos. Chem. Phys., 12, 261–269, doi:10.5194/acp-12-261-2012, 2012.

Oye, H. A., Mason, N., Peterson, R. D., Richards, N. E., Rooy, E. L., Stevens McFadden, F. J., Zabreznik, R. D., Williams, F. S., and Wagstaff, R. B.: Aluminum: Approaching the new millennium, JOM, 51, 29–42, doi:10.1007/s11837-999-0207-3, 1999.

Peters, G. P., Marland, G., Le Quéré, C., Boden, T., Canadell, J. G., and Raupach, M. R.: Rapid growth in CO_2 emissions after the 2008-2009 global financial crisis, Nature Climate Change, 2, 2–4, doi:10.1038/nclimate1332, 2012.

Prinn, R. G., Weiss, R. F., Krummel, P. B., O'Doherty, S., Fraser, P. J., Mühle, J., Reimann, S., Vollmer, M. K., Simmonds, P. G., Maione, M., Arduini, J., Lunder, C. R., Schmidbauer, N., Young, D., Wang, H. J., Huang, J., Rigby, M., Harth, C. M., Salameh, P. K., Spain, T. G., Steele, L. P., Arnold, T., Kim, J., Hermansen, O., Derek, N., Mitrevski, B., and Langenfelds, R.: The ALE / GAGE / AGAGE Network (DB1001), Carbon Dioxide Information Analysis Center (CDIAC), Oak Ridge National Laboratory, doi:10.3334/CDIAC/atg.db1001, 2016.

Rigby, M., Ganesan, A. L., and Prinn, R. G.: Deriving emissions time series from sparse atmospheric mole fractions, J. Geophys. Res., 116, D08306, doi:10.1029/2010JD015401, 2011.

Rigby, M., Prinn, R. G., O'Doherty, S., Montzka, S. A., McCulloch, A., Harth, C. M., Mühle, J., Salameh, P. K., Weiss, R. F., Young, D., Simmonds, P. G., Hall, B. D., Dutton, G. S., Nance, D., Mondeel, D. J., Elkins, J. W., Krummel, P. B., Steele, L. P., and Fraser, P. J.: Re-evaluation of the lifetimes of the major CFCs and CH_3CCl_3 using atmospheric trends, Atmos. Chem. Phys., 13, 2691–2702, doi:10.5194/acp-13-2691-2013, 2013.

Rigby, M., Prinn, R. G., O'Doherty, S., Miller, B. R., Ivy, D., Mühle, J., Harth, C. M., Salameh, P. K., Arnold, T., Weiss, R. F., Krummel, P. B., Steele, L. P., Fraser, P. J., Young, D., and Simmonds, P. G.: Recent and future trends in synthetic greenhouse gas radiative forcing, Geophys. Res. Lett., 41, 2623–2630, doi:10.1002/2013GL059099, 2014.

Rommelaere, V., Arnaud, L., and Barnola, J.: Reconstructing recent atmospheric trace gas concentrations from polar firn and bubbly ice data by inverse methods, J. Geophys. Res., 102D, 30069–30083, 1997.

Rubino, M., Etheridge, D. M., Trudinger, C. M., Allison, C. E., Battle, M. O., Langenfelds, R. L., Steele, L. P., Curran, M., Bender, M., White, J. W. C., Jenk, T. M., Blunier, T., and Francey, R. J.: A revised 1000 year atmospheric δ^{13}C-CO_2 record from Law Dome and South Pole, Antarctica, J. Geophys. Res., 118, 1–18, doi:10.1002/jgrd.50668, 2013.

Schaefer, H., Petrenko, V. V., Brook, E. J., Severinghaus, J. P., Reeh, N., Melton, J. R., and Mitchell, L.: Ice stratigraphy at the Pâkitsoq ice margin, West Greenland, derived from gas records, J. Glaciol., 55, 411–421, doi:10.3189/002214309788816704, 2009.

Schmitt, J., Seth, B., Köhler, P., Willenbring, J., and Fischer, H.: Atmospheric CF_4 trapped in polar ice – A new proxy for granite weathering, in: Goldschmidt Conference, Mineral. Mag., 77, 2160, available at: http://epic.awi.de/34102/, 2013.

Smith, A. M., Levchencko, V. A., Etheridge, D. M., Lowe, D. C., Hua, Q., Trudinger, C. M., Zoppi, U., and Elcheikh, A.: In search of in-situ radiocarbon in Law Dome ice and firn, Nucl. Instrum. Meth. B, 172, 610–622, 2000.

Sowers, T., Bernard, S., Aballain, O., Chappellaz, J., Barnola, J., and Marik, T.: Records of the δ^{13}C of atmospheric CH_4 over the last 2 centuries as recorded in Antarctic snow and ice, Global Biogeochem. Cy., 19, GB2002, doi:10.1029/2004GB002408, 2005.

Sturges, W. T., McIntyre, H. P., Penkett, S. A., Chappellaz, J., Barnola, J., Mulvaney, R., Atlas, E., and Stroud, V.: Methyl bromide, and other brominated methanes, and methyl iodide in polar firn air, J. Geophys. Res., 106, 1595–1606, 2001.

Sturrock, G. A., Etheridge, D. M., Trudinger, C. M., Fraser, P. J., and Smith, A. M.: Atmospheric histories of halocarbons from analysis of Antarctic firn air: Major Montreal Protocol species, J. Geophys. Res., 107, 4765, doi:10.1029/2002JD002548, 2002.

Tabereaux, A. T.: Anode effects, PFCs, global warming, and the aluminum industry, JOM, 46, 30–34, doi:10.1007/BF03222629, 1994.

Thompson, R. L., Gerbig, C., and Rödenbeck, C.: A Bayesian inversion estimate of N_2O emissions for western and central Europe and the assessment of aggregation errors, Atmos. Chem. Phys., 11, 3443–3458, doi:10.5194/acp-11-3443-2011, 2011.

Trudinger, C. M., Enting, I. G., Etheridge, D. M., Francey, R. J., Levchenko, V. A., Steele, L. P., Raynaud, D., and Arnaud, L.: Modeling air movement and bubble trapping in firn, J. Geophys. Res., 102, 6747–6763, 1997.

Trudinger, C. M., Etheridge, D. M., Rayner, P. J., Enting, I. G., Sturrock, G. A., and Langenfelds, R. L.: Reconstructing atmospheric histories from measurements of air composition in firn, J. Geophys. Res., 107, 4780, doi:10.1029/2002JD002545, 2002.

Trudinger, C. M., Enting, I. G., Rayner, P. J., Etheridge, D. M., Buizert, C., Rubino, M., Krummel, P. B., and Blunier, T.: How well do different tracers constrain the firn diffusivity profile?, Atmos. Chem. Phys., 13, 1485–1510, doi:10.5194/acp-13-1485-2013, 2013.

Tsai, W.-T., Chen, H.-P., and Hsien, W.-Y.: A review of uses, environmental hazards and recovery/recycle technologies of perfluorocarbons (PFCs) emissions from the semiconductor

manufacturing processes, J. Loss Prevent. Proc., 15, 65–75, doi:10.1016/S0950-4230(01)00067-5, 2002.

U.S. Geological Survey: Aluminium statistics, last modification: 1 April 2014, compiled by: Buckingham, D. A., Plunkert, P. A., and Bray, E. L., available at: http://minerals.usgs.gov/minerals/pubs/historical-statistics/, last access: 5 October 2014.

Vogel, H. and Friedrich, B.: Development and Research Trends of the Neodymium Electrolysis – A Literature Review, in: Proceedings of the 8th European Metallurgical Conference, Düsseldorf, 2015.

Vollmer, M. K., Mühle, J., Trudinger, C. M., Rigby, M., Montzka, S. A., Harth, C. M., Miller, B. R., Henne, S., Krummel, P. B., Hall, B. D., Young, D., Kim, J., Arduini, J., Wenger, A., Yao, B., Reimann, S., O'Doherty, S., Maione, M., Etheridge, D. M., Li, S., Verdonik, D. P., Park, S., Dutton, G., Steele, L. P., Lunder, C. R., Rhee, T. S., Hermansen, O., Schmidbauer, N., Wang, R. H. J., Hill, M., Salameh, P. K., Langenfelds, R. L., Zhou, L., Blunier, T., Schwander, J., Elkins, J. W., Butler, J. H., Simmonds, P. G., Weiss, R. F., Prinn, R. G., and Fraser, P. J.: Atmospheric histories and global emissions of halons H-1211 ($CBrClF_2$), H-1301 ($CBrF_3$), and H-2402 ($CBrF_2CBrF_2$), J. Geophys. Res.-Atmos., 121, 3663–3686, doi:10.1002/2015JD024488, 2016.

Weiler, K.: On the Composition of Firn Air and its Dependence on Seasonally Varying Atmospheric Boundary Conditions and the Firn Structure, PhD thesis, University of Bern, 2008.

Witrant, E. and Martinerie, P.: Input Estimation from Sparse Measurements in LPV Systems and Isotopic Ratios in Polar Firns, in: Proceedings of the 5th IFAC Symposium on System Structure and Control, Grenoble, France, 4–6 February 2013, 654–659, available at: http://www.gipsa-lab.grenoble-inp.fr/~e.witrant/papers/13_ifac_firn.pdf (last access: July 2014), 2013.

Witrant, E., Martinerie, P., Hogan, C., Laube, J. C., Kawamura, K., Capron, E., Montzka, S. A., Dlugokencky, E. J., Etheridge, D., Blunier, T., and Sturges, W. T.: A new multi-gas constrained model of trace gas non-homogeneous transport in firn: evaluation and behaviour at eleven polar sites, Atmos. Chem. Phys., 12, 11465–11483, doi:10.5194/acp-12-11465-2012, 2012.

Wong, D. S., Fraser, P., Lavoie, P., and Kim, J.: PFC emissions from detected versus nondetected anode effects on the aluminium industry, JOM, 67, 342–353, doi:10.1007/s11837-014-1265-8, 2015.

Worton, D. R., Sturges, W. T., Gohar, L. K., Shine, K. P., Martinerie, P., Oram, D. E., Humphrey, S. P., Begley, P., Gunn, L., Barnola, J., Schwander, J., and Mulvaney, R.: Atmospheric trends and radiative forcing of CF_4 and C_2F_6 inferred from firn air, Environ. Sci. Technol., 41, 2184–2189, 2007.